I&EC research
Industrial & Engineering Chemistry Research

pubs.acs.org/IECR
Article

Dry Reforming of Methane over Rare-Earth Metal Oxide Ni−M−Al (M = Ce, La) Catalysts

Alua Manabayeva,* Päivi Mäki-Arvela, Zuzana Vajglová, Mark Martinez-Klimov, Olha Yevdokimova, Anssi Peuronen, Mika Lastusaari, Teija Tirri, Kaisar Kassymkan, Tolkyn S. Baizhumanova, Manapkhan Zhumabek, Rabiga O. Sarsenova, Zauresh T. Zheksenbaeva, Gulnar N. Kaumenova, Vincenzo Russo, Dmitry Yu. Murzin,* and Svetlana A. Tungatarova

Cite This: *Ind. Eng. Chem. Res.* 2023, 62, 20588−20607

Read Online

ACCESS | Metrics & More | Article Recommendations | Supporting Information

ABSTRACT: Dry reforming of methane (DRM) was investigated using Ni−M oxide catalysts prepared by solution combustion synthesis (SCS) and compared with Ni/α-Al_2O_3 synthesized by impregnation. According to X-ray diffraction, fresh oxide Ni−La and Ni−Ce catalysts displayed low crystallinity, which was improved after DRM, accompanied by the appearance of metallic Ni. Ni−Ce−Al and Ni−La−Al catalysts formed, respectively, $CeAlO_3$ and $LaAlO_3$ phases during the reaction. For studied catalysts featuring low surface areas ranging from 3 to 12 m^2/g, the average metal particle sizes were 12−32 nm according to transmission electron microscopy, with the particles growing larger with time-on-stream (TOS) apart from Ni−α-Al_2O_3. DRM tests were conducted for different TOSs, demonstrating that the highest CH_4 transformation rate was concomitant with the highest deactivation rate during 30 min of time-on-stream. The most stable performance in temperature stability experiments was demonstrated by the Ni−Ce−Al catalyst, for which, similar to other catalysts, the H_2/CO ratio remained close to unity. In long-term stability tests, the Ni−Ce−Al catalyst displayed a 3.1-fold higher turnover frequency (TOF) compared with Ni−α-Al_2O_3, with no significant deactivation. The TOF values were comparable to the literature, highlighting the potential of SCS as an alternative approach for synthesis of DRM catalysts.

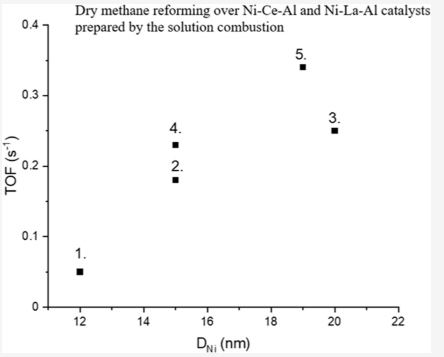

INTRODUCTION

Currently the contribution of energy produced from fossil fuels is declining because of the more widespread utilization of alternative energy sources. One such potential alternative energy source is hydrogen, which can be produced from natural gas as well as biogas and carbohydrates. Fuel cells in particular are the most promising devices for energy and heat generation requiring high-purity hydrogen.[1]

Generation of hydrogen from biogas containing methane is viewed as a viable option, which can compete with conventional technologies based on natural gas. There are three possible technologies of methane reforming: dry reforming (DRM), steam reforming, and partial oxidation.[2] It has been suggested in ref 3 that the most suitable process to utilize biogas composed of CH_4 and CO_2 is the dry reforming process. The reaction is highly endothermic (ΔH_{298} = +247 kJ/mol), producing synthesis gas with a H_2/CO molar ratio equal to 1:1.

In fact, during DRM, several side reactions (eqs 1−3) can also occur,[4] with some of them being exothermic and proceeding at temperatures below 530 °C

Boudouard reaction: $2CO \leftrightarrow C+CO_2$;

$$\Delta H_{298} = -172.4 \text{ kJ/mol} \quad (1)$$

hydrogenation of CO_2: $CO_2+2H_2 \leftrightarrow C + 2H_2O$;

$$\Delta H_{298} = -90 \text{ kJ/mol} \quad (2)$$

hydrogenation of CO: $CO+H_2 \leftrightarrow C+H_2O$;

$$\Delta H_{298} = -131.3 \text{ kJ/mol} \quad (3)$$

The following reactions (eqs 4 and 5) are favored at high temperatures[4]

methane decomposition: $CH_4 \leftrightarrow C + 2H_2$;

$$\Delta H_{298} = +74.9 \text{ kJ/mol} \quad (4)$$

Received: July 10, 2023
Revised: October 27, 2023
Accepted: October 30, 2023
Published: November 20, 2023

https://doi.org/10.1021/acs.iecr.3c02341
Ind. Eng. Chem. Res. 2023, 62, 20588−20607

reverse water − gas-shift(RWGS)

$$: CO_2 + H_2 \leftrightarrow CO + H_2O; \qquad \Delta H_{298} = +41\ \text{kJ/mol} \tag{5}$$

Several catalysts have been investigated in DRM comprising supported noble[5] and transition metals.[6] The main benefit in using transition-metal catalysts, such as supported Ni, is that the metals are abundant and inexpensive. On the other hand, especially supported nickel catalysts are prone to deactivation, which can be mitigated at least partially by fine-tuning the catalyst composition. For example, CeO_2 and La_2O_3 have been intensively tested as promoters or supports for Ni,[7−10,12−17,19,21,22] while other modifications involve the use of encapsulated Ni nanoparticles[11] or mesoporous supports for Ni[18] as well as modifications with iron.[20] The main idea has been to suppress the sintering of Ni and coking with these methods. For example, Ni supported on halloysite clay and promoted with Co, Ce, or La resulted in improved catalyst stability by suppressing metal sintering during DRM.[8]

Ceria-promoted catalysts have been promising in DRM. An overview of different catalysts tested in DRM is demonstrated in Table S1. Ceria promoted 5 wt % Ni on CeO_2−Al_2O_3 [with the molar ratio of Ce/(Ce + Al) of 0.1, denoted as 5Ni−CeAl], producing a CH_4 conversion of 60% and CO_2 conversion of 79% (Table S1, entry 1),[16] and remained stable over 40 h. As a comparison, nonreduced Ni/CeO_2 (denoted as 5 wt % Ni/CeO_2-NR, where NR—nanorods) exhibited higher activity than 5 wt % Ni/CeO_2-NP (NP—nanopolyhedra) and higher stability over 30 h. In the case of 5 wt % Ni/CeO_2-NR, the initial conversion of CH_4 and CO_2 was 81 and 85%, respectively, with a H_2/CO ratio of 1.1 (Table S1, entries 2, 3).[17] Ce-promoted Ni-based catalysts can prevent formation of $NiAl_2O_4$, which can otherwise decrease catalytic activity.[9] It was shown that 3 wt % Ce on Ni/Al_2O_3 enhanced catalytic activity and stability toward coke formation in methane reforming.[10] In addition, a mixed oxide $Ce_{1-x}Ni_xO_2$ catalyst exhibited high activity and strong resistance to coke deposition,[11] while Ni/Al_2O_3 and Ni/CeO_2 catalysts deactivated rapidly due to nickel sintering and coke formation.[12,13] According to[14], 10 wt % Ni/Al_2O_3 catalyst contained the $NiAl_2O_4$ phase, while enhanced activity in DRM was obtained for the catalyst with the addition of 5 wt % CeO_2, forming $CeAlO_3$ and, thereby, enhancing the carbon resistance of the catalyst. In addition, dry reforming at low temperatures has also been investigated.[15] For Ni/SiO_2, the CH_4 and CO_2 conversions are very low and not stable, which can be contributed to carbon formation (approximately 24%) on large Ni^0 particles. Ni−Ce/SiO_2 was more active than Ni−Ce/γ-Al_2O_3. The methane conversion level reached an equilibrium (60%), while for Ni−Ce/γ-Al_2O_3, the CO_2 conversion was higher.

Lanthana-modified Ni/Al_2O_3[21] and the use of Ni/La_2O_3[7] have shown promising results in DRM. For example, 8 wt % La was added to 33 wt % Ni/Al_2O_3, giving higher catalytic performance and stability compared to other catalysts with lower and higher La loadings (Table S1, entry 6).[21] A comparison of different lanthanides as a support for nickel was performed in model biogas dry reforming at a space velocity of 200,000 mL g_{cat}^{-1} h^{-1}.[7] The results showed that Ni/La_2O_3 and Ni/Sm_2O_3 exhibited the highest conversion rates for both CH_4 and CO_2 reactants, and the maximum conversion values were achieved at 750 °C (approximately 52%).[23] The best performance was observed for Ni/La_2O_3, in which the $LaNiO_3$ perovskite structure was formed.[7] Although CeO_2 and PrO_x possess larger redox activity and oxygen mobility, the catalytic activity of Ni/CeO_2 and Ni/PrO_x catalysts was significantly lower in comparison to that of Ni/La_2O_3 and Ni/Sm_2O_3. It was stated in[19] that the addition of La_2O_3 to Ni/Al_2O_3 can decrease the acidity of the catalyst and prevent the formation of pyrolytic carbon because the basic La_2O_3 favored chemisorption and dissociation of CO_2 and subsequently accelerated carbon elimination by the reverse Boudouard reaction $CO_2 + C = 2CO$. Another advantage of La_2O_3 addition was its capability to efficiently disperse Ni crystallites in Al_2O_3 and prevent the growth of Ni grains at high temperatures. Furthermore, it was reported in ref 19 that incorporation of La_2O_3 and CeO_2 in Ni/Al_2O_3 increased conversion of CH_4 and CO_2, as well as the yields of H_2 and CO and their selectivity.

As a comparison, the Ni catalyst supported onto a commercial alumina gave initial conversion values of CH_4 and CO_2 of 50 and 60%, respectively, decreasing thereafter, while the H_2/CO ratio remained constant for 20 h (Table S1, entry 4).[18] In contrast, the 15Ni−5Fe−30Al catalyst exhibited good performance during DRM in spite of its high acidity.[20] In addition, even if the surface area of Ni−Fe−Al was the lowest among other catalysts demonstrated in Table S1, it was highly active and stable for 20 h (Table S1, entry 5).

Solution combustion synthesis (SCS) is a very simple method allowing fast preparation of materials, which can be used as ceramic powders for a variety of technologies, including catalysts, gas sensors, and ceramic pigments.[24] SCS catalysts, in particular, have been applied in partial oxidation of methane,[25] DRM,[26] and aqueous hydrogenation of maleic acid.[27] Metal nitrate hydrates [$M(NO_3)_x \cdot nH_2O$] are used as oxidizers, and urea (glycine, etc.) is used as a fuel in the SCS.[28] Metal nitrate hydrates and urea are mixed with deionized water. This solution undergoes a combustion at a preignition temperature (500 °C in the current work). SCS consists of self-sustaining exothermic interactions between metal nitrate hydrates and fuel that are intimately blended at the molecular level, displaying characteristics similar to those of other flammable systems.

The exothermic reaction of $Al(NO_3)_3 \cdot 9H_2O$ and urea is shown as

$$2Al(NO_3)_3 \cdot 9H_2O + 5CH_4N_2O = Al_2O_3 + 8N_2 + 5CO_2 + 28H_2O$$

As can be seen, the gas release occurs, removing nitrogen and carbon from dinitrogen and carbon dioxide as well as leading to the release of water. In the end, only metals in different forms remained: oxide, alloy, spinel, and so forth.

Such a preparation method has been coined SCS. In an alternative option (the combustion method per se), metal nitrates, hydrates, and fuel are thoroughly stirred to obtain a gel, which is thereafter placed into a furnace. One more example of the combustion method is a case when the metal nitrates and fuel are dissolved in water and stirred at 90 °C on an electric heater and the formed gel is burnt at 500 °C or other temperatures.

The aim of this work was to demonstrate for the first time the activity and stability of the rare-earth element-promoted Ni−Al catalysts prepared by the solution combustion method in dry methane reforming. The performance of the catalysts was evaluated with a time-on-stream (TOS) of 30−40 min at each temperature and their thermal stability was tested in a

https://doi.org/10.1021/acs.iecr.3c02341
Ind. Eng. Chem. Res. 2023, 62, 20588−20607

stepwise manner. For some selected catalysts, long-time stability was also investigated. Thermodynamic limitations were investigated by taking into account the equilibrium conversion. Several physicochemical methods including powder X-ray diffraction (XRD), transmission electron microscopy (TEM), temperature-programmed techniques, scanning electron microscopy with elemental analysis (SEM−EDX), and CHNS analysis were used to correlate catalyst performance with their properties and to study the coke formation in the spent catalysts.

EXPERIMENTAL PART

Catalyst Synthesis. The catalysts were prepared by SCS. The necessary amounts of the metal nitrates $Ni(NO_3)_2{\cdot}6H_2O$, $Al(NO_3)_3{\cdot}9H_2O$, $La(NO_3)_3{\cdot}6H_2O$, $Ce(NO_3)_3{\cdot}9H_2O$, and urea were placed in a thermostable beaker and completely dissolved in 30 mL of deionized water, which was heated beforehand to 80 °C. The beaker containing the solution was placed in a muffle furnace preheated to 500 °C (an exception was 15Ni−15Ce−20La, which required 550 °C). The combustion of the solution occurred within 10−15 min, and thereafter, the beaker was cooled to room temperature.

A monometallic Ni/α-Al_2O_3 catalyst was prepared by impregnation to compare its performance with the catalysts synthesized by SCS. The α-Al_2O_3 support with a grain size of 0.04−0.08 mm was obtained by the calcination of γ-Al_2O_3 in the furnace at 1150 °C for 2 h.[29] Thereafter, a certain amount of $Ni(NO_3)_2{\cdot}6H_2O$ was dissolved in water and mixed with α-Al_2O_3, followed by drying at 250 °C for 1.5 h and calcination at 650 °C for 3 h. The loading amount of Ni was fixed at 12 wt % to have a comparable metal loading.

Catalyst Characterization. The phase composition and structure of the synthesized catalysts were characterized by powder XRD with a DRON-4-0.7 diffractometer using CoKα radiation in the range of 2θ = 5−100°.

Temperature-programmed reduction with hydrogen was carried out using MicrotracBelcat II equipment. For each analysis, ca. 100 mg of a sample was pretreated at 200 °C for 2 h with argon. Thereafter, the sample was cooled to 50 °C and heated up to 800 °C with a temperature ramping rate of 10 °C/min under a H_2/Ar atmosphere (5 vol % H_2 and 95 vol % Ar) using 1.5 and 28.5 mL/min H_2 and Ar flows, respectively. The target temperature was maintained for 20 min.

Temperature-programmed desorption (NH_3-TPD) experiments were carried out on the same instrument. Ca. 60−100 mg of the catalyst sample was pretreated at 500 °C for 1 h. Thereafter, a sample was cooled to 50 °C. Ammonia was preadsorbed at 100 °C for 30 min, and thereafter, the physisorbed ammonia was flushed from the catalyst surface for 60 min under a helium flow. In the following step, the sample was heated to 600 °C at a ramp rate of 10 °C/min under 1.5 mL/min of ammonia and 28.5 mL/min of helium, respectively (5 vol % NH_3 and 95 vol % He); the target temperature-maintaining time was 20 min.

Temperature-programmed desorption was performed to determine the concentration of basic sites using AutoChem 2010 (Micrometrics). At the first step, the catalyst with ca. 200 mg was dried at 150 °C for 30 min under He (AGA, 99.996%), after which it was cooled to 100 °C. Subsequently, CO_2 adsorbed on the catalyst surface for 30 min and was flushed from the catalyst surface at 100 °C for 30 min. Finally, the temperature was elevated to 700 °C at a ramp rate of 10 °C/min.

CHNS measurements were conducted using a Thermo Fisher Scientific Flash 2000 Organic Elemental Analyzer equipped with a TC detector. The temperature in the furnace was 950 °C. As standards, several organic compounds, such as methionine, cystine, 2,5-bis(5-*tert*-butyl-benzoxazol-2-yl) thiophene, and sulfanilimide, were used.

SEM analysis was performed using a Zeiss Leo Gemini 1530 Scanning Electron Microscope equipped with a Thermo Scientific UltraDry Silicon Drift Detector (SDD).

Thermogravimetric analysis (TGA) and differential thermal analysis (DTA) were performed with an SDT Q600 apparatus (TA Instruments) under a N_2 or air atmosphere (flow rate 100 mL/min) and the temperature was increased to 800 °C at a heating rate of 10 °C/min.

TEM analysis was performed with a JEOL JEM-1400Plus instrument giving a resolution of 0.38 nm and using an acceleration voltage of 120 kV and an OsisQuemesa 11 Mpix bottom-mounted digital camera to investigate the metal particle size and textural characteristics. The catalysts were reduced using the following reduction program: 450 °C was reached at a ramp rate of 10 °C/min and maintained as the target temperature for 2 h. Determination of the metal particle sizes was performed with ImageJ software.

A Micromeritics 3Flex-3500 instrument was used to evaluate the textural properties. The moisture in the catalyst samples was removed, and the samples (0.15 g) were degassed ex situ under vacuum at 180 °C for 20 h. Thereafter, a sample was pretreated in the physisorption equipment under 0.2−0.3 bar at 180 °C for 5 h, followed by liquid nitrogen adsorption at −196 °C and various relative pressures. The BET and DFT methods were used to calculate the specific surface area and pore size distribution, respectively.

Catalytic Experiments. The catalytic activity tests were performed under atmospheric pressure, using 2 mL of a catalyst in a fixed-bed quartz reactor (the internal reactor diameter and the length of the catalytic bed are 20 and 5 mm, respectively). This catalyst amount was chosen to reach such values of conversion that would allow a meaningful interpretation of the data. The catalyst particles were placed on a layer of quartz wool. The catalyst performance was evaluated based on the mass of nickel used in the experiments. The catalyst without the inert material dilution was introduced in the reactor to monitor catalyst deactivation within TOS (30 min and 10 and 20 h on stream), as reported in.[30] A short-term stability test was performed as follows: the temperature range was set from room temperature to 650 °C, maintained for 2 min, and increased thereafter to 750 °C and maintained for 2 min again. At 850 °C, the holding time was 30 min. The stability test at the temperature range of 600−900 °C was done in steps of 50 °C that were maintained for 10 min at each step. In addition, long-term stability tests were performed with one catalyst at 850 °C for 7 h and continued over two additional days for 7 and 6 h of TOS.

The model biogas mixture with a gas ratio of CH_4/CO_2/Ar equal to 1:1:1 (vol) was used in DRM.[31] The total flow rate of gases was 100 mL/min, corresponding to a gas hourly space velocity (GHSV) of 3000 h^{-1}. The reduction was conducted before an experiment only for 15Ni−15Ce−20La at a H_2 flow rate of 40 mL/min at 900 °C for 20 min. Thereafter, the reactor with the catalyst was flushed with Ar at a flow rate of 70 mL/min for 30−40 min. No special activation of other Ni catalysts, including 12% Ni/Al_2O_3, was done before catalytic experiments. The gas composition of the reactants and

https://doi.org/10.1021/acs.iecr.3c02341
Ind. Eng. Chem. Res. 2023, 62, 20588−20607

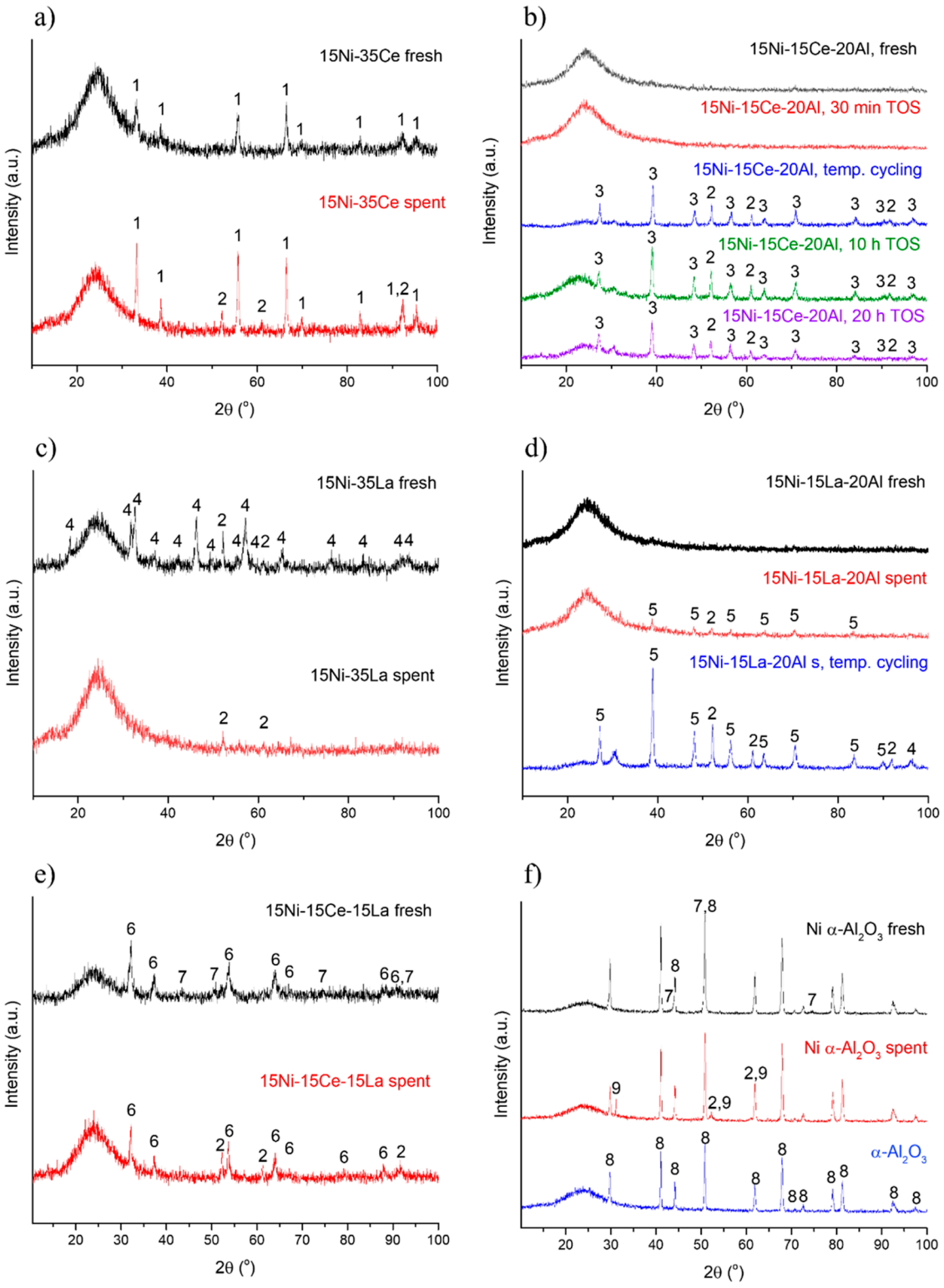

Figure 1. XRD patterns of fresh and spent catalysts (TOS = 30 min): (a) 15Ni−35Ce, (b) 15Ni−15Ce−20Al, (c) 15Ni−35La, (d) 15Ni−15La−20Al, (e) 15Ni−15Ce−20La, and (f) fresh and spent 12 wt % Ni/α-Al_2O_3. The spent catalysts were used in DRM for 30 min at 850 °C with a GHSV of 3000 h^{-1}, spent; (b) 15Ni−15Ce−20Al, (d) 15Ni−15La−20Al, and (e) 15Ni−15Ce−20La catalysts were also used in DRM in the temperature range of 600−900 °C and back to 600 °C; (b) 15Ni−15Ce−20Al and (f) 12 wt % Ni/α-Al_2O_3 in a long-term experiment were used in DRM at 850 °C for two consecutive runs with 5 h of TOS. Conditions: V_{cat} = 2 mL, GHSV = 3000 h^{-1}, 100 mL/min. Explanation of phases: 1. CeO_2, 2. Ni^0, 3. $CeAlO_3$, 4. $La(OH)_3$, 5. $LaAlO_3$, 6. $La_2Ce_2O_7$, 7.NiO, 8. α-Al_2O_3, and 9. CeO_x (x = 1.695).

products was analyzed using a gas chromatograph equipped with a TCD (thermal conductivity detector), as described in detail below.

Analysis. Analysis of the initial mixture and reaction products was carried out using a chromatograph with Chromos software. The chromatograph was equipped with packed and

https://doi.org/10.1021/acs.iecr.3c02341
Ind. Eng. Chem. Res. 2023, 62, 20588−20607

capillary columns. CH_4, CO_2, and CO were analyzed with a capillary column using a FID, while H_2, oxygen, and nitrogen were analyzed by a packed column with a TCD. The temperature of the TCD was 200 °C, while the evaporator temperature was set at 280 °C, and the temperature of the column was 40 °C. The flow rate of Ar was 10 mL/min.

Definitions. Conversion of CH_4 and CO_2 (X), the consumption rates (r), and the space-time yields of CO and H_2 (STY), as well as the H_2/CO ratio were calculated as below (eqs 6−13)

$$X_{CH_4} = \frac{(F_{CH_4,in} - F_{CH_4,out})}{F_{CH_4,in}} \times 100\% \quad (6)$$

$$X_{CO_2} = \frac{(F_{CO_2,in} - F_{CO_2,out})}{F_{CO_2,in}} \times 100\% \quad (7)$$

$$r_{CH_4} = \frac{F_{CH_4,in} - F_{CH_4,out}}{m_{Ni}} \quad (8)$$

$$r_{CO_2} = \frac{F_{CO_2,in} - F_{CHO_2,out}}{m_{Ni}} \quad (9)$$

$$TOF_{CH_4} = \frac{F_{CH_4,in} - F_{CH_4,out}}{n_{Ni,exp}} \quad (10)$$

In which $n_{Ni,exp}$ denotes the moles of the exposed metal. The mean Ni particle size obtained from TEM was used in the calculations.

$$STY_{H_2} = \frac{F_{H_2,out}}{m_{Ni}} \quad (11)$$

$$STY_{CO} = \frac{F_{H_2,out}}{m_{Ni}} \quad (12)$$

$$H_2/CO = \frac{STY_{H_2}}{STY_{CO}} \quad (13)$$

F_i denotes the molar flow of gas i (mol/s).

The carbon balance has been calculated, as defined in ref 32, as follows

$$carbonbalance = \frac{F_{CH_4,out} + F_{CO_2,out} + F_{CO,out}}{F_{CH_4,in} + F_{CO_2,in}} \quad (14)$$

The experiments were performed in the absence of external mass transfer limitations, and the Weisz−Prater parameter φ, calculated from

$$\varphi = \frac{r_{obs} r_p^2 RT}{p_{CH_4} D_{eff}} \leq 1 \quad (15)$$

was found to be 0.14 for the long-term experiment at 850 °C and 1 atm over the 15Ni−15Ce−20Al catalyst, indicating that the internal mass transfer limitations can be neglected. The following input data were used for the calculation: the binary diffusivity for methane and carbon dioxide $D_{AB} = 1.69 \times 10^{-4}$ m^2/s according to the Chapman−Enskog equation[33] and Knudsen diffusivity $D_K = 6.90 \times 10^{-6}$ m^2/s for methane in the 15Ni−15Ce−20Al catalyst with a pore radius of 8.5 nm (determined by BJH for the desorption branch of the N_2 physisorption isotherm). The effective diffusion coefficient was calculated from the Bosanquet equation to be D_e of 6.63×10^{-6} m^2/s. Effective diffusivity was obtained from eq 16

$$D_{eff} = \frac{\varepsilon}{\tau} D_e \quad (16)$$

with the value for porosity divided by tortuosity $\frac{\varepsilon}{\tau}$ equal to 0.1 giving $D_{eff} = 6.63 \times 10^{-7}$ m^2/s.

Methods for Thermodynamic Analysis. The equilibrium composition of the methane dry reforming reaction network was computed using the Gibbs reactor module implemented in ChemCAD software.[34] The nonideality of the system was taken into account adopting the Soave−Redlich−Kwong equation of state, as suggested in the literature.[35] The computations were conducted by fixing a total pressure of 1 bar and a feed composition of 1:1:1 CO_2, CH_4, and Ar.

RESULTS AND DISCUSSION

Characterization of Catalysts. *XRD Results.* The recorded powder XRD patterns are shown in Figure 1. Metallic Ni (henceforth Ni^0) [PDF 01-071-4655] appears as peaks at ca. 52.5, 61.4, and 92.4° 2θ in most of both fresh and spent catalysts. Ni^0 originate from the reduction of Ni^{2+} during catalyst preparation[36−39] and/or in the spent catalysts used for the dry reforming process.[18]

The XRD profile of bimetallic 15Ni−35Al was shown in the previous study.[20] The bimetallic 15Ni−35Al exhibited only amorphous features, while the amorphous content in 15Ni−35Ce appears to be rather large (Figure 1a). In the latter, CeO_2 [PDF 00-067-0122] could be identified as the only crystalline phase in the fresh catalyst. The crystallinity of the catalyst tested in DRM for 30 min of TOS at 850 °C is slightly higher, and in addition to CeO_2, crystalline Ni^0 is clearly present. The fresh 15Ni−15Ce−20Al catalyst shows a high degree of amorphous content and very low crystallinity. The few very weak peaks could signify the presence of the cubic phase of $CeAlO_3$ [PDF 00-028-0260], but no reliable analysis could be carried out.[40] The spent catalyst is equally amorphous, while peaks of Ni^0 are barely distinguishable from those in the background. No reflexes of the CeO_2 phase were distinguished in 15Ni−15Ce−20Al.

When this catalyst was used in a long-term stability test (Figure 1b), increasing temperature and holding for 30−40 min at each temperature, the $CeAlO_3$ phase, with a better fit to peaks with a tetragonal unit cell [PDF 01-081-1186] than cubic, was formed together with Ni^0, as confirmed with the main peaks at 25, 39.2, 48.5, 56.6, and 70.9° 2θ of $CeAlO_3$. Formation of cerium aluminate occurred above 600 °C during DRM. Analogously, after reduction at 850 °C, CeO_2 was reduced completely to $CeAlO_3$.[40−42] It was reported in ref 37 that formation of Ce_2O_3 is possible above 800 °C, as shown in eq 17

$$2CeO_2 + H_2 \rightarrow Ce_2O_3 + H_2O \quad (17)$$

and Ce^{III} oxide can further react with Al_2O_3 (eq 18)

$$Ce_2O_3 + Al_2O_3 \rightarrow 2CeAlO_3 \quad (18)$$

The spent 15Ni−15Ce−20Al catalyst evaluated in the stability test at 850 °C for 10 h shows a reflex at 2θ ca. 30.5°, becoming more prominent after 20 h of TOS. This peak could correspond to the main peak of the CeO_x (x = 1.695) phase [PDF 04-018-6657] (not listed in Figure 1). Because

https://doi.org/10.1021/acs.iecr.3c02341
Ind. Eng. Chem. Res. 2023, 62, 20588−20607

many other catalysts also display this peak, it may also arise from Al_2O_3 with a low crystallinity.

The fresh catalyst 15Ni−35La exhibited a $La(OH)_3$ phase [PDF 01-083-4962] and Ni^0. The former phase disappeared during DRM (Figure 1c), judging from the XRD pattern of the spent catalyst. Typically, synthesized lantana prepared from lanthanum nitrate via, for example, the precipitation method using ammonium hydroxide as a precipitant contains both La_2O_3 and $La(OH)_3$ after calcination at 700 °C since lantana is hydroxylated to lanthanum hydroxide (eq 19)

$$La_2O_3 + 3H_2O \rightarrow 2La(OH)_3 \quad (19)$$

However, in the presence of humidity[43] and in the current case, no lantana was observed. It was also reported in ref 44 that $La(OH)_3$ is decomposed under an inert or oxygen atmosphere to La_2O_3 at 800 °C, which was not observed in this work. Analogously, the spent catalyst (30 min TOS) has at least Ni^0, while other crystalline phases were not present. For the fresh 15Ni−15La−20Al catalyst, no significant crystalline phases have been apparent from the XRD pattern. The few that barely emerge from the background could correspond to the perovskite structure of $LaAlO_3$ at 39.0, 48.3, 56.4, 70.7, and 83.8° 2θ (Figure 1d) [PDF 01-083-4233], as also reported in.[45] This phase is more clearly present, accompanied by Ni^0, in the spent 15Ni−15La−20Al catalyst used in DRM at 850 °C for 30 min of TOS. The XRD data revealed that in the current case, during DRM between 600 and 900 °C in the temperature cycling experiment, the $LaAlO_3$ phase remained stable, while the relative amounts of the crystalline phases have significantly increased compared to the amorphous content. Furthermore, a qualitative comparison to the short-term DRM test shows that the relative amounts of $LaAlO_3$ and Ni^0 remained the same. As reported in ref 46, perovskite-type structures with the unit formula of ABO_3 can be formed during the polymeric steric entrapment method, which allows us to prepare high-entropy alloys. In ref 47, perovskites were prepared by the coprecipitation method at a temperature of 550 °C.

As a comparison, the fresh 15Ni−15Ce−20La contained cubic $La_2Ce_2O_7$ [PDF 01-084-4175] (or CeO_2 due to their similar unit cell dimensions) and NiO [PDF 04-006-6160], while in the spent catalyst, the NiO phase disappeared and Ni^0 appeared instead (Figure 1e). The $La_2Ce_2O_7$ phase can be formed during heating of La_2O_3 and CeO_2 at 800 °C for several hours,[48] and thus, it is also feasible that this phase was formed during the SCS.

In addition, a monometallic reference catalyst, 12 wt % Ni/α-Al_2O_3, was analyzed by XRD. The fresh catalyst contained mostly pure α-Al_2O_3 [PDF 01-075-1862], while peaks of NiO can also be distinguished from the XRD pattern, some of them overlapping with the peaks of the α-Al_2O_3 phase. In comparison with the current work in ref 49, α-alumina was mixed with some amounts of θ-alumina, showing the impurity of the support. Furthermore, in ref 50, Ni was highly dispersed in the support, and after calcination at 700 °C, Ni/γ-Al_2O_3 became α-Al_2O_3 and $NiAl_2O_4$, which was not identified in the current case because Ni did not react with Al_2O_3. During DRM, NiO was reduced to Ni^0, which is difficult to determine reliably as the peaks of α-Al_2O_3 and ceria overlap with the Ni^0 reflexes.

XRD analyses of the fresh catalysts reduced at 850 °C is presented in Figure S1. XRD data of the reduced catalysts showed reflexes with high intensity, while for nonreduced catalysts, it was difficult to visually identify any reflexes for 15Ni−15Ce−20Al and 15Ni−15La−20Al catalysts (Figure 1). After reduction of the catalysts at 850 °C, it can be seen that NiO in 15Ni−15Ce−20Al was not completely reduced, since NiO species remained; however, the intensity of the NiO reflexes is low. On the other hand, no NiO was visible in other catalysts (Figure S1). Nonreduced 15Ni−15Ce−20La and 12 wt % Ni/α-Al_2O_3 catalysts (Figure 1) had small reflexes corresponding to NiO, which was transformed to metallic Ni after reduction. Ce- and La-aluminates $CeAlO_3$ and $LaAlO_3$ as well as lanthanum cerate, $La_2Ce_2O_7$, remained stable after reduction.

SEM−EDX Results. The results from elemental analysis of the fresh and some spent catalysts (Table S2) show that nickel content in the bimetallic catalysts was ca. 17 wt % except in 15Ni−35Al, where it reached 42 wt %, as reported in the previous study.[20] In trimetallic catalysts, the Ni amounts varied in the range of 24−26 wt %. The molar ratio of Ni/M (M = Ce, La) was in the range of 1.3−1.4, while in bimetallic catalysts, this ratio was between 0.6 and 0.8, remaining nearly the same in the fresh and spent catalysts, even if Ni was located on the tips of carbon nanotubes in several catalysts (see below).

TEM Results. It was difficult to identify metal particles in the fresh catalysts due to a low contrast (Figure 2a,b), while in the spent catalyst with a TOS of 30 min at 850 °C, the metal particles were clearly identified. Thus, the metal particle size distribution was calculated only for the spent catalysts (Table 1). The smallest average metal particle size was observed in the spent 15Ni−35Al (not shown in Table 1), while slightly larger particle sizes were observed in the other bimetallic catalysts containing alkali metals.[20] The trimetallic catalyst 15Ni−15Ce−20Al exhibited smaller particles in comparison to 15Ni−15La−20Al.

In the TEM images of all of the spent catalysts, the carbon nanotubes can be easily detected. For example, carbon nanotubes with a diameter of 70−90 nm can be found in the current work in the spent 15Ni−15La−20Al. In ref 51, carbon nanotubes of between 10 and 23 nm in size were found, when the average size of Ni species was 7−8 nm. However, after temperature cycling, the average size of the catalyst particles was increased to 32 nm, indicating possible sintering. As a comparison with[52], graphitic coke was detected on Ni−CeO_2 catalysts after the reaction; however, in the current case, this type of coke was not identified in the XRD pattern of either Ni−Ce or Ni−Ce−Al catalysts. Moreover, in ref 52, Ni species were well-dispersed on Ce−Al support. As can be seen from Table 1, the average size of metal particles is 15 nm for both 15Ni−35Ce and 15Ni−15Ce−20Al, which corresponds to the literature. The average metal particle size was not significantly affected by the temperature cycling exposure for 15Ni−15Ce−20Al. However, sintering of nickel particles occurred for 15Ni−15Ce−20La, and the nickel particle size increased to 32 nm.

As a comparison, two different types of Ni−Al catalysts were investigated. One, 15Ni−35Al, was synthesized via the SCS method, while the other one, 12 wt % Ni/α-Al_2O_3, was prepared by the impregnation method. 15Ni−35Al exhibited the smallest particle size after DRM compared to their trimetallic counterparts (Table 1). In addition, the average Ni particle size of 12 wt % Ni/α-Al_2O_3 was 9 nm for the fresh catalyst (not shown in Table 1), while the spent catalyst has a particle size of 15 nm, the same as 15Ni−35Ce and 15Ni−

https://doi.org/10.1021/acs.iecr.3c02341
Ind. Eng. Chem. Res. 2023, 62, 20588−20607

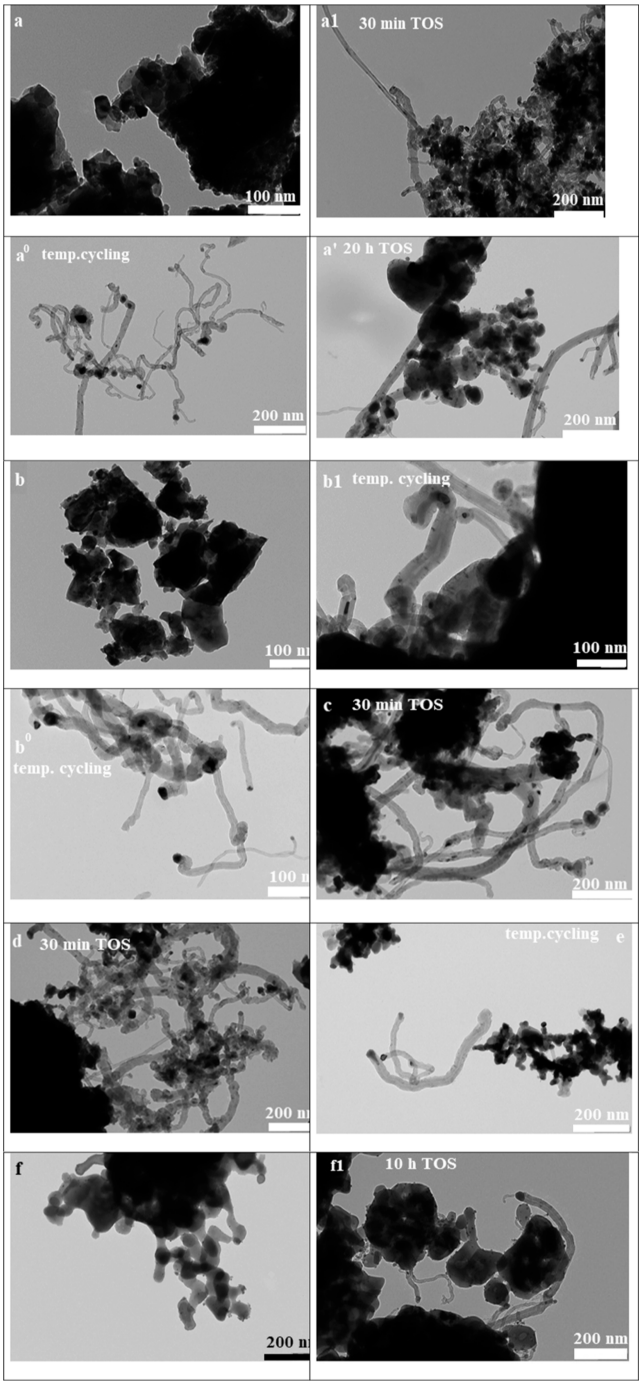

Figure 2. TEM images of (a)15Ni−15Ce−20Al fresh, (a1) 15Ni−15Ce−20Al after 30 min of TOS, (a^0) 15Ni−15Ce−20Al after temperature cycling at 600−900−600 °C, (a′) 15Ni−15Ce−20Al after 20 h of TOS, (b) 15Ni−15La−20Al fresh, (b1) 15Ni−15La−20Al spent, (c) 15Ni−35Ce spent, (d) 15Ni−35La spent, (e) 15Ni−15Ce−20La after temperature cycling at 600−900−600 °C, (f) 12 wt % Ni/α-Al_2O_3 fresh, and (f1) 12 wt % Ni/α-Al_2O_3 spent. a1, b1, c1, and d1 spent catalysts used in DRM for 30 min at 850 °C, a^0 in temperature cycling at 600−900−600 °C, a′—20 h of TOS, and f1—10 h with a GHSV of 3000 h^{-1}.

15Ce−20Al tested in 30 min of TOS. Small metal particle sizes for Ni−Al catalysts have also been reported in the literature as being in the range of 4−11 nm, with the average particle size being 7 nm.[18] In another work,[45] Ni/α-Al_2O_3 obtained via impregnation with the addition of carbon black in the

Table 1. TEM Analysis of the Fresh and Spent Catalysts[a]

catalyst	spent metal particle size (nm)
15Ni−15Ce−20Al	[c]15,[d]18,[f]23
15Ni−15La−20Al	[c]19,[d]32
15Ni−15Ce−20La	[d]26
15Ni−35Ce	[c]15
12 wt % Ni/α-Al_2O_3	[e]15
15Ni−35La	[c]20
15Ni−35Al	[b]12

[a]The spent catalysts were used in DRM for 30 min at 850 °C with a GHSV of 3000 h^{-1}. [b]From ref 20, Ni particle size. [c]30 min of TOS. [d]Temperature cycling experiment at 600−900−600 °C. [e]10 h of TOS at 850 °C. [f]20 h of TOS at 850 °C.

intermediate steps exhibited metal particles of a size in the range of 10−25 nm. It was stated that the difference in the particle sizes of different Ni−Al catalysts directly depends on their surface areas. Another reason can be attributed to Ni sintering caused by calcination of catalysts at high temperatures (1300 °C). However, in the current work, no sintering was observed for 12 wt % Ni/α-Al_2O_3 despite using 1150 °C for preparation of α-Al_2O_3.

Textural Properties. The N_2 adsorption/desorption isotherms and pore size distributions are shown in Table 2. According to the IUPAC classification, the isotherms of all catalysts can be categorized as type IV with H3 hysteresis loops, which is related to mesoporous materials with wedge-shaped pores. The specific surface areas of the catalysts prepared by solution combustion methods are very small and the catalysts contain more mesopores than micropores. The specific surface area of the spent catalysts decreased by 37−58%, and at the same time, the ratio of microporous to mesoporous volume decreased due to carbon accumulation. The specific surface area of the spent catalyst 15Ni−35La was only 42% of the fresh one, while for the other catalysts, the corresponding levels were 50% for 15Ni−35Ce < 15Ni−15La−20Al (60%) < 15Ni−15Ce−20Al (63%), indicating that the latter catalyst retained the majority of its surface area.

Ammonia TPD Results. The results from ammonia TPD showed that the highest acidity was observed in a bimetallic 15Ni−35Al catalyst, as expected due to the presence of a high amount of alumina (Figure 3 and Table 3). The trimetallic 15Ni−15Ce−20Al exhibited 27% lower acidity than 15Ni−15La−20Al due to its slightly higher Al content (Table S1). All three catalysts contained more strong acid sites, that is, those with the temperature maximum for ammonia desorption peaks close to 600 °C. The α-Al_2O_3 and γ-Al_2O_3 supports have Lewis acid sites determined by pyridine-FTIR.[53] While Ni/α-Al_2O_3 could exhibit Lewis acid sites, from NH_3-TPD, the amount of NH_3 desorbed from α-Al_2O_3 was negligible. This could be related to a much lower surface area of α-Al_2O_3 compared to that of γ-Al_2O_3.

Furthermore, the acid/base ratio of the Ni/α-Al_2O_3 (nonpromoted) catalyst was 2.63, higher than that for 3 wt % La−20 wt % Ni/77 wt % α-Al_2O_3 catalyst, indicating that there was electron deficiency at the interface of the metal and the support.[54] The type of acidity of Ni/α-Al_2O_3 was also Lewis.

Results from CO_2 TPD. The strength of basic sites is defined as weak when CO_2 desorption (Figure 4 and Table 4) occurs below 200 °C, as medium when CO_2 desorption occurs between 200 and 400 °C, as strong when CO_2 desorption

https://doi.org/10.1021/acs.iecr.3c02341
Ind. Eng. Chem. Res. 2023, 62, 20588−20607

Table 2. Textural Properties of the Fresh and Spent Catalysts[a,b]

catalyst	F/S	S_{BET} (m^2/g)	V_{tot} (cm^3/g)	V_μ (<2 nm) (cm^3/g)	V_m (<20 nm) (cm^3/g)	V_μ/V_m (-)
15Ni−15Ce−20Al	F	8	0.011	0.003	0.007	0.43
15Ni−15Ce−20Al	S	5	0.018	0.001	0.008	0.13
15Ni−15La−20Al	F	5	0.008	0.002	0.006	0.33
15Ni−15La−20Al	S	3	0.014	0	0.006	0
15Ni−35Ce	F	10	0.024	0.002	0.011	0.18
15Ni−35Ce	S	5	0.020	0.001	0.006	0.16
15Ni−35La	F	12	0.050	0	0.004	0
15Ni−35La	S	5	0.020	0.001	0.007	0.14
15Ni−35Al[20]	n.d	n.d	n.d	n.d	n.d	n.d
15Ni−35Al[20]	F	8	0.014	0.004	0.011	0.33

[a]The spent catalysts were used in DRM for 30 min at 850 °C with a GHSV of 3000 h^{-1}. Notation: F, fresh; S, spent. [b]n.a., not available; n.d., not determined.

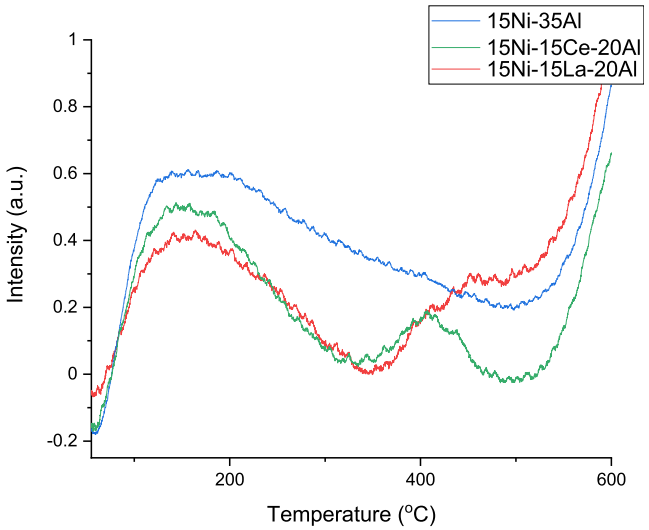

Figure 3. Ammonia TPD profiles for some catalysts prepared by the solution combustion method.

Table 3. Results from Ammonia TPD for Some Catalysts Prepared by the Solution Combustion Method[a]

catalyst	$T_{1,max}$ (°C)	$T_{2,max}$ (°C)	$T_{3,max}$ (°C)	normalized area/g_{cat}
15Ni−15Ce−20Al	159	401	622	0.54
15Ni−15La−20Al	146	439	622	0.65
15Ni−35Al[20]	140	922	n.a	1

[a]n.a., not available.

occurs between 400 and 600 °C, and as very strong when CO_2 desorption occurs above 600 °C.[55]

The highest basicity was recorded for 15Ni−35La, followed by 15Ni−35Ce. The 15Ni−35La catalyst contained the $La(OH)_3$ phase according to XRD, and this phase has a high concentration of medium-strength basic sites with the peak desorption maximum at 410 °C,[56] which is rather close to the peak maximum for 15Ni−35La in the current case. For trimetallic catalysts, 15Ni−15Ce−20Al exhibited more basic sites at high temperature (ca. 528 °C) in comparison to 15Ni−15La−20Al, and it was more stable in DRM. This result is in accordance with[56] where $Ni/CeO_2-Al_2O_3$ exhibited more strong basic sites in comparison to $Ni/Al_2O_3-La_2O_3$.

Hydrogen TPR. TPR patterns of the Ni−based catalysts are depicted in Figure 5 and Table 5. The reduction of Ni species starts at a higher temperature for 15Ni−35Al than for alkali-modified Ni-catalysts. The TPR results of 15Ni−15Ce−20Al showed that nickel species in the catalysts were reduced in the temperature range between 300 and 400 °C.[57] The first peak at 300 °C corresponds to the reduction of Ni^{2+} (NiO) species on the catalyst surface, which is in line with XRD results showing the presence of metallic nickel. The TPR peak in the temperature range of 400−500 °C can be explained by the reduction of NiO species strongly interacting with the support (15Ni−15La−20Al). It should be pointed out, however, that the presence of NiO was not visible in the current case in XRD. In case of 15Ni−15Ce−20Al, it is also possible that some CeO_2 species are reduced on the surface to Ce^{3+}, as reported in[37]. When comparing the TPR results of 15Ni−15Ce−20Al with its XRD results, it can, however, be seen that the crystallinity for this catalyst is very low, thus indicating that based on TPR and XRD results, it is difficult to clearly separate different species.

CHNS Analysis. CHNS results of the spent catalysts used in DRM for 30 min at 850 °C with a GHSV of 3000 h^{-1} show that the normalized carbon content per mass of nickel decreased for 15Ni−15La−20Al > 15Ni−35La >15Ni−15Ce−20Al > 15Ni−35Ce > 15Ni−35Al (Table 6 and Figure 6). The normalized carbon content of the Ni−Ce−Al catalyst was higher than that of Ni−Ce catalysts due to the presence of Al and the higher acidity of the former catalyst (Table 4). The reason is the contribution of CeO_2, which enhances adsorption of CO_2 in the interfacial region and, at the same time, decreases carbon formation.[58] It has been reported in the literature[42] that Ce-promoted catalysts enhance CH_x gasification and formation of CO when CeO_2 is reduced to CeO_{2-x} and thereafter reoxidized back to CeO_2 in the presence of CO_2. As a comparison, CHNS analysis was also performed for the 15Ni−15Ce−20Al catalyst used under the same conditions for 20 h of TOS and its carbon content was 3.8-fold that for the catalyst used only for a TOS of 30 min. Moreover, the former catalyst exhibited a molar H/C ratio of 0.1, indicating that the H/C ratio decreased when the catalyst was exposed for a long TOS.

The amount of coke increased with the increasing metal particle size of the spent catalyst, and at the same time, the molar ratio H/C exhibited a minimum. The H/C ratio was very low for NiLa, with relatively large metal particles. When the H/C ratio is below 2, it indicates the presence of aromatic coke, while a value below 1 denotes more dehydrogenated coke.

TGA. According to TGA (Figure 6), the normalized amount of carbon calculated per exposed catalyst decreased for 15Ni−

https://doi.org/10.1021/acs.iecr.3c02341
Ind. Eng. Chem. Res. 2023, 62, 20588−20607

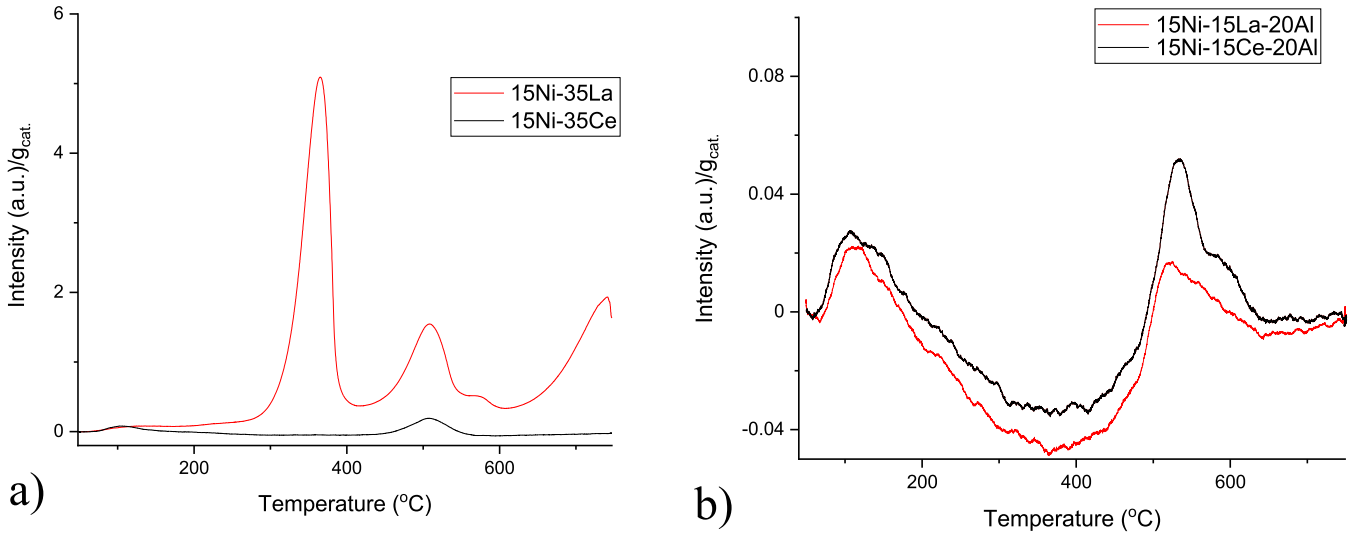

Figure 4. Results from the CO_2 TPD.

Table 4. Results from CO_2 TPD

catalyst	$T_{1,max}$ (°C)	$T_{2,max}$ (°C)	$T_{3,max}$ (°C)	normalized area/g_{cat}
15Ni−15Ce−20Al	101	528	n.a	0.04
15Ni−15La−20Al	115	518	n.a	0.05
15Ni−35Ce	106	508	n.a	0.07
15Ni−35La	364	509	741	1

15La−20Al (56 wt %/g_{cat}) > 15Ni−15Ce−20Al (21 wt %/g_{cat}). The same order was observed by CHNS analysis, as described above. The maximum of heat release observed at 575 °C pointed out on the filamentous type of coke formation observed also over nickel catalysts supported on mixed oxides Fe/Mg-bearing metallurgical waste[59] and FeNi/H−Y-5.1.[60] Furthermore, TGA of the fresh catalysts in the presence of air revealed phase transformations for 15Ni−15Ce−20Al (5.3 wt %) > 15Ni−15La−20Al (3.2 wt %). The weight increase in the TGA profile is due to oxidation of metallic nickel and/or ceria found in the spent catalyst analogously reported in[61]. Under nitrogen, the weight loss for 15Ni−15La−20Al was higher at 500 °C, while oxidation of this catalyst occurred under air.

Table 5. Results from Hydrogen TPR

catalyst	$T_{1,max}$ (°C)	$T_{2,max}$ (°C)	$T \geq 3_{max}$ (°C)	normalized area
15Ni−15Ce−20Al	320	377	800	0.33
15Ni−15La−20Al	380	542	no	1.0
15Ni−15Ce−20La	372	527	no	0.19
15Ni−35Ce	248	340	540	0.91
15Ni−35La	194	363	397, 574, 620, 694	0.31
15Ni−35Al[20]	353	456	800	0.37
12 wt % Ni−α/Al_2O_3	375	527	no	0.02

However, at 800 °C, the weight loss for this catalyst was much smaller than that under air.

THERMODYNAMIC ANALYSIS

The calculated composition in terms of molar fractions is reported in Figure 7.

As revealed, hydrogen is the main product already at temperatures higher than 620 °C. The methane fraction is

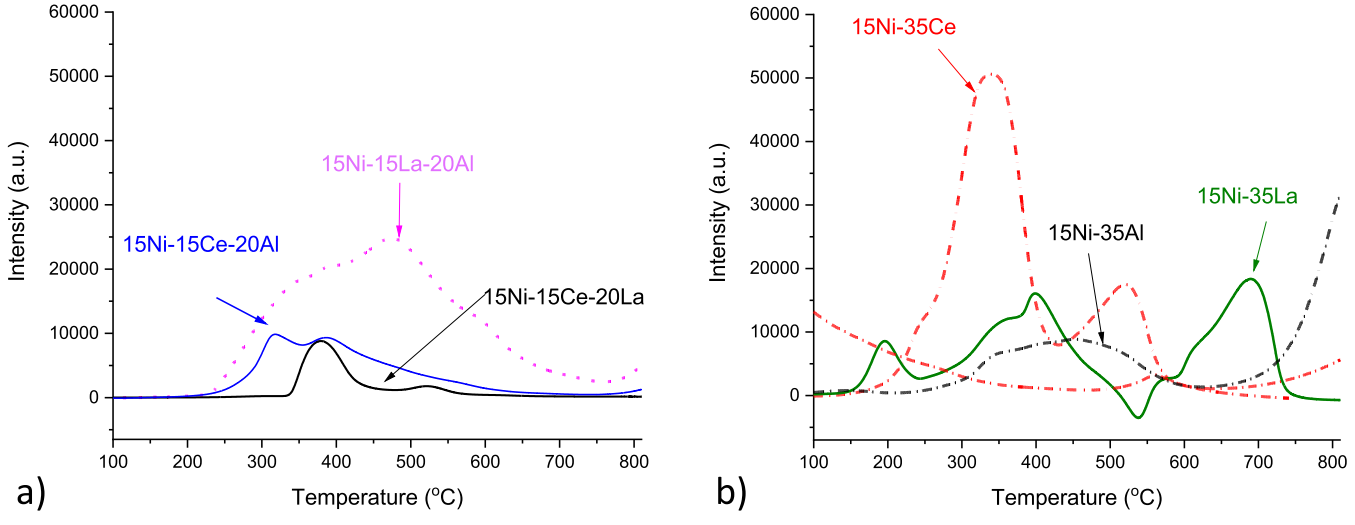

Figure 5. Hydrogen TPR of different (a) trimetallic and (b) bimetallic catalysts.

https://doi.org/10.1021/acs.iecr.3c02341
Ind. Eng. Chem. Res. 2023, 62, 20588−20607

Table 6. Normalized Carbon Content Determined from CHNS Analysis from the Spent Catalysts Used in DRM at 850 °C for 30 min of TOS

catalyst	normalized carbon content (wt %)/g_{Ni}	H/C molar ratio
15Ni−15Ce−20Al	0.38	0.22
15Ni−15La−20Al	1.0	0.13
15Ni−35Ce	0.39	0.23
15Ni−35La	0.61	0.25
15Ni−35Al[20]	0.12	0.26

decreasing with temperature, approaching full conversion. The CO fraction becomes higher at high temperatures. The trends are well in line with the ones reported in the literature.[35]

CATALYTIC RESULTS

Comparison of the Performance of Different Catalysts. Evaluation of catalytic behavior at short TOSs (TOS = 30 min) of different catalysts in DRM was done at 850 °C. Data on hydrogen consumption in TPR and normalized carbon formation in the spent catalysts, plotted as a function of methane and CO_2 transformation rates, are shown in Figure 8 and Table 7. The methane and CO_2 transformation rates calculated per gram of nickel decreased as follows: 15Ni−15La−20Al > 15Ni−15Ce−20Al > 15Ni−35La >15Ni−35Ce > 15Ni−35Al. The high activity for 15Ni−15La−20Al can be explained by its high hydrogen consumption in TPR.[62] This catalyst also exhibited the highest amount of coke calculated per exposed Ni.

The amount of formed coke correlated well with the methane transformation rate for all other catalysts except 15Ni−35Ce, as described in the section on TGA. Furthermore, the highest carbon formation was observed in 15Ni−15La−20Al, featuring, according to XRD, $La(OH)_3$ not being stable during DRM. Analogously to the current case with the La-

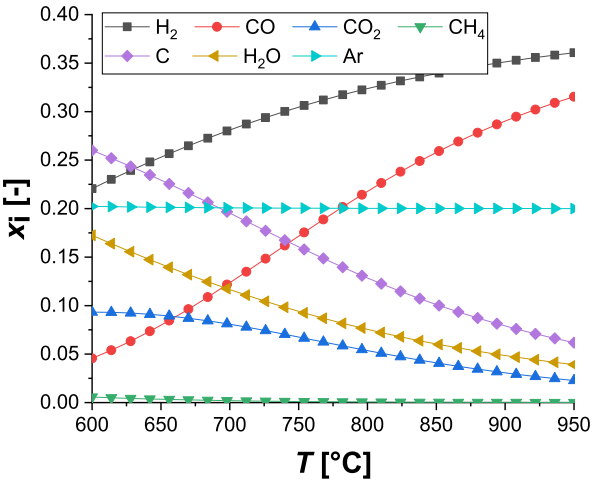

Figure 7. Equilibrium composition of the reaction mixture as a function of temperature.

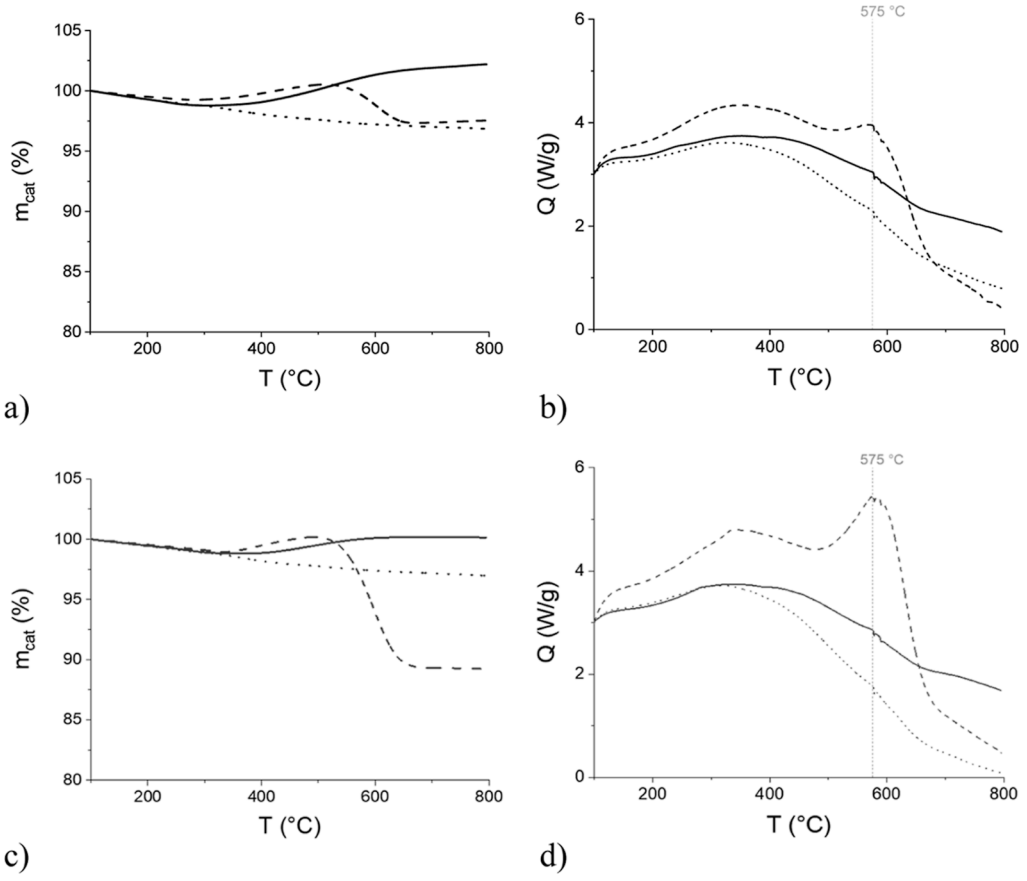

Figure 6. Mass of the catalyst and heat release as a function of temperature during TGA for (a,b) 15Ni−15Ce−20Al and (c,d) 15Ni−15La−20Al catalysts. Conditions: to 800 °C with 10 °C/min in 100 mL/min of gas flow. Legend: fresh catalyst in N_2 flow (dot−dot line), fresh catalyst in air flow (solid line), and spent catalyst in air flow (dash−dash line). The spent catalysts were used at 850 °C in DRM for 30 min of TOS.

https://doi.org/10.1021/acs.iecr.3c02341
Ind. Eng. Chem. Res. 2023, 62, 20588−20607

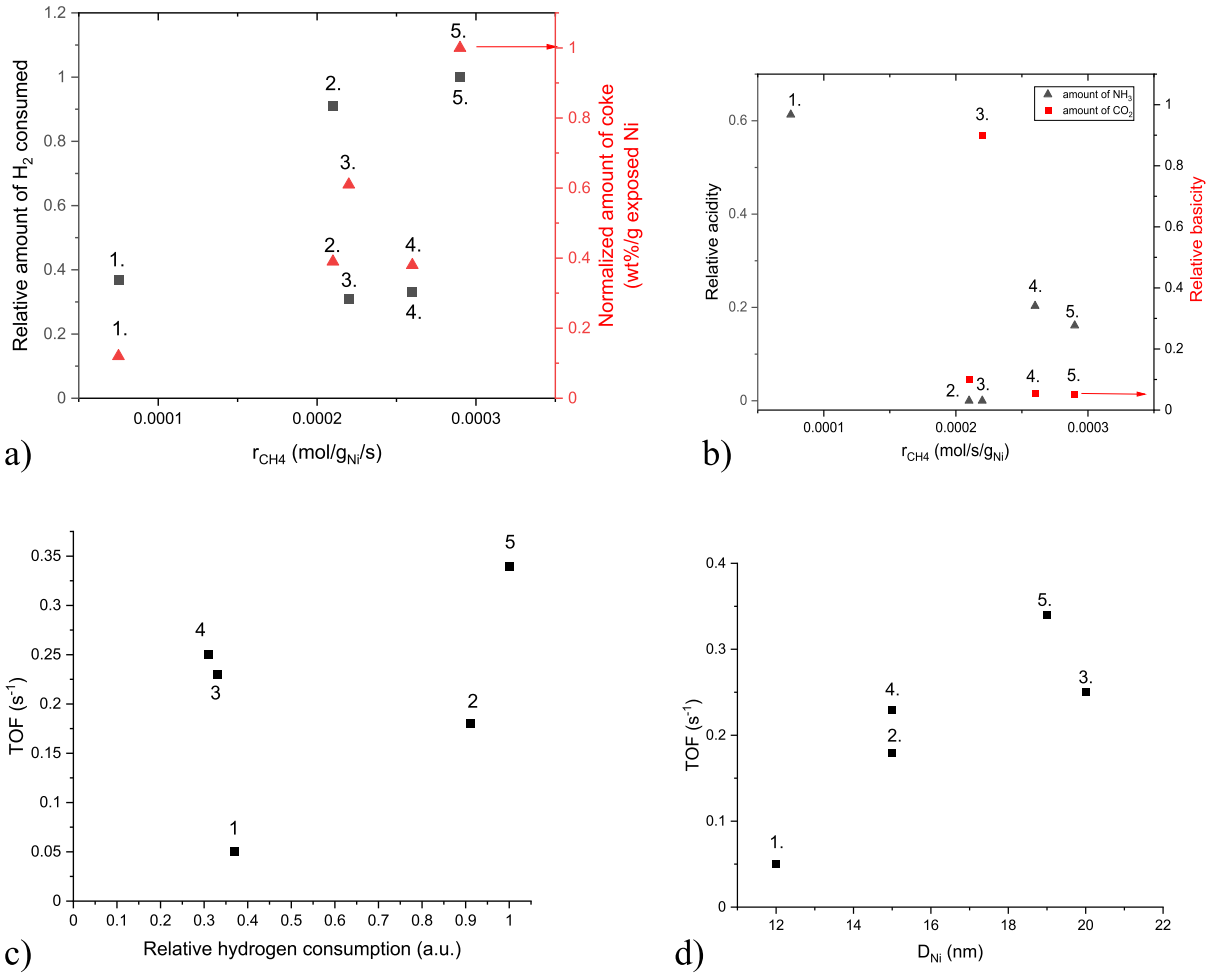

Figure 8. (a) Relative consumed hydrogen from TPR and normalized amount of coke and (b) relative acidity/basicity as a function of the methane transformation rate at 850 °C after 30 min of TOS in DRM, (c) initial TOF calculated from methane transformation as a function of relative hydrogen consumption in TPR, and (d) average Ni particle size. Notation: 1. 15Ni−35Al, 2. 15Ni−35Ce, 3. 15Ni−35La, 4. 15Ni−15Ce−20Al, and 5. 15Ni−15La−20Al.Conditions: $CH_4/CO_2/Ar$ = 1:1:1, 850 °C, 30 min of TOS, GHSV = 3000 h^{-1}, 2 mL of catalyst, and a gas flow rate of 100 mL/min.

Table 7. Methane and CO_2 Transformation Rates, Initial TOF Calculated from Methane Conversion, STYs, H_2/CO Ratio, Carbon Balance, and Deactivation Rate from the Short-term DRM (TOS = 30 min) at 850 °C

catalyst	r_{CH_4} ($mol/g_{Ni}/s$)	r_{CO_2} ($mol/g_{Ni}/s$)	TOF_{CH_4} (s^{-1})	$rate_{CH_4}/rate_{CO_2}$	STY_{H_2} ($mol/g_{Ni}/s$)	STY_{CO} ($mol/g_{Ni}/s$)	CB (%)	deactivation rate %/min/g_{cat}[a]	H_2/CO
15Ni−15Ce−20Al	2.6×10^{-4}	2.1×10^{-4}	0.23	1.3	4.5×10^{-4}	3.0×10^{-4}	67	0	1.5
15Ni−15La−20Al	2.9×10^{-4}	2.6×10^{-4}	0.34	1.1	5.6×10^{-4}	4.0×10^{-4}	79	0.20	1.4
15Ni−35Ce	2.1×10^{-4}	1.7×10^{-4}	0.18	1.2	3.8×10^{-4}	2.4×10^{-4}	68	0.1	1.6
15Ni−35La	2.2×10^{-4}	1.9×10^{-4}	0.25	1.2	4.0×10^{-4}	2.7×10^{-4}	70	0.005	1.5
15Ni−35Al	0.75×10^{-4}	0.70×10^{-4}	0.05	1.1	1.5×10^{-4}	1.0×10^{-4}	74	0.03	1.5

[a]Deactivation rate is calculated during the decrease in CH_4 conversion per time and mass of the catalyst.

modified catalyst containing more carbon than the corresponding Ce-modified catalysts 15Ni−15Ce−20Al, the La-modified Ni−halloysite catalyst showed higher coking than Ce−Ni halloysite.[8] In the current case, the Ce-modified catalyst exhibited a molar ratio of Ni/Ce of 1.35 (Table S1), while no coking was observed in ref 16 with the spent Ni−Ce−alumina catalyst, with a Ni/Ce molar ratio of 1.6 and a nickel particle size of 10 nm after DRM at 800 °C.

The bimetallic 15Ni−35Al catalyst displayed the slowest methane transformation rate (Figure 8a) due to the strong interactions of Ni with the support, resulting in low reducibility of the nickel (Figure 5).

The Ni−Ce catalyst exhibited the second slowest methane transformation rate despite its easy reducibility at a low temperature (Figure 5) and exhibited high hydrogen consumption in TPR (Table 5). The amount of coke per nickel was low as, most probably, the presence of the CeO_2 phase (Figure 1a) aided in coke suppression (see section TGA Analysis). On the other hand, its trimetallic counterpart, 15Ni−15Ce−20Al with a low crystallinity (Figure 1b), was less reducible than 15Ni−35Ce (Table 5), nevertheless exhibiting a slightly higher methane transformation even with a low acidity. For the other lanthanum catalyst, the bimetallic 15Ni−35La was rather active in DRM (Table 7) although it was not stable

https://doi.org/10.1021/acs.iecr.3c02341
Ind. Eng. Chem. Res. 2023, 62, 20588−20607

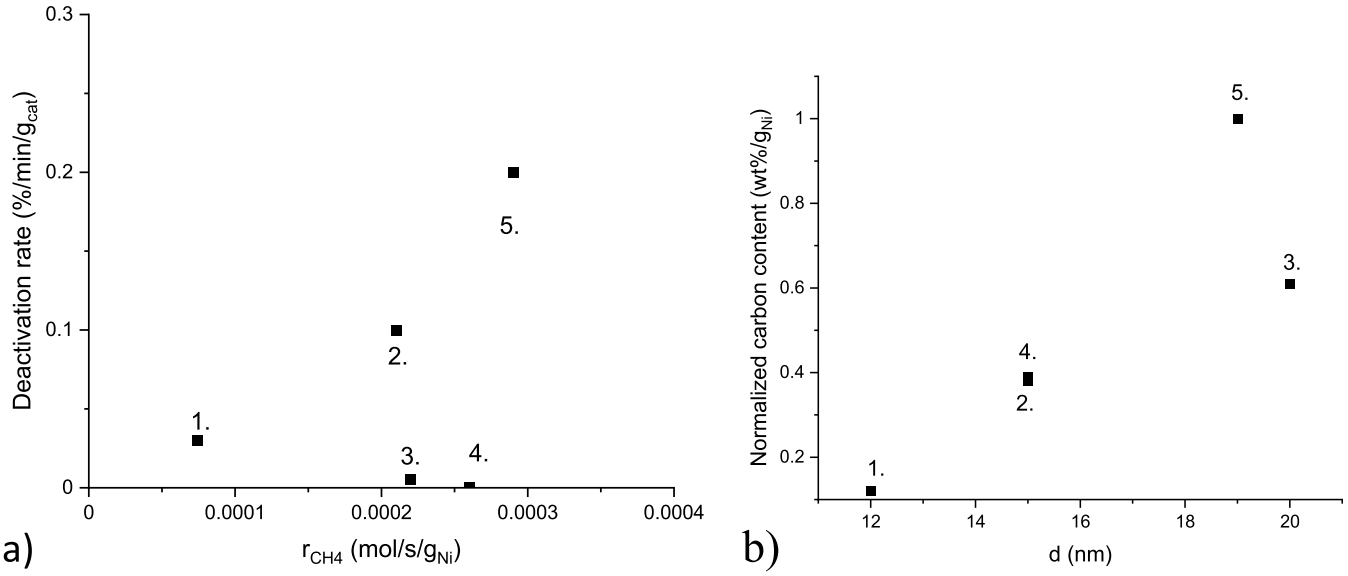

Figure 9. (a) Deactivation rate as a function of methane transformation at 850 °C after 30 min of TOS in DRM. (b) Normalized carbon content in the spent catalyst as a function of Ni particle size in the spent catalyst. Notation: 1. 15Ni−35Al, 2. 15Ni−35Ce, 3. 15Ni−35La, 4. 15Ni−15Ce−20Al, and 5. 15Ni−15La−20Al. Conditions: $CH_4/CO_2/Ar$ = 1:1:1, 850 °C, 30 min of TOS, GHSV = 3000 h^{-1}, 2 mL of catalyst, and a gas flow rate of 100 mL/min.

during DRM at 850 °C, as can be concluded from Figure 1c. The $La(OH)_3$ phase, confirmed by XRD, decomposed during DRM, and the area of metallic nickel also decreased. Although it was easily reduced already at a low temperature, the reducibility of 15Ni−35La was low and comparable with that of 15Ni−35Al. The 15Ni−35La catalyst was also the most basic, which, however, did not suppress the coke formation significantly (Figure 2c).

Initial turnover frequencies (TOFs) calculated from methane transformation for different catalysts did not correlate with relative hydrogen consumption (Figure 9c). However, TOFs were increasing with increasing metal particle size and reaching the maximum for 15Ni−15La−20Al, while for 20 nm Ni particles observed in 15Ni−35La, the TOF value dropped. In addition, structure sensitivity for methane transformation was also observed, where a volcano-type curve to the methane turnover frequency was obtained with increasing Ni particle size.[63]

The deactivation rate was the highest for 15Ni−15La−20Al (Table 7), which contained the second-largest metal particle in the spent catalyst (Figure 9b and Table 2). The normalized carbon content per exposed amount of nickel increased with increasing nickel particle size in the spent catalyst, except for 15Ni−35La (Figure 9b). Analogous results showing high coke formation with large Ni particles for Ni supported on the silica catalyst in steam reforming of methane at 800 °C were obtained in refs 63 and 64 as well as in DRM over Ni−CeO_2 modified with different metals.[65] Also, in DRM, more coke was formed over larger Ni particles.[37] It should be pointed out here that the direct comparison between Ni particle size and coking of five different catalysts in this study is not fully straightforward because the support is not the same for these catalysts with different metal particle sizes. The TEM image of the spent 15Ni−15La−20Al revealed that nickel is encapsulated into the carbon nanofiber opposite for 15Ni−15Ce−20Al (Figure 1). Analogously, Ni particles were trapped into filaments during DRM for 8 wt % Ni−Al−La.[66] Over the 15Ni−15La−20Al catalyst, the CO_2 conversion rate was 2.9 × 10^{-4} mol/g_{Ni}/s, while methane conversion was 2.6 × 10^{-4} mol/g_{Ni}/s due to the presence of La giving basicity to the catalyst (Table 3). In the current case, this catalyst had a Ni/Al molar ratio of 0.85 (Table S2) and contained perovskite-type mixed La−Ni−Al oxide (Figure 1). This ratio is quite high when compared to[67], when the optimal molar ratio of Ni/Al was 0.42 in $LaNi_xAl_{1-x}O_3$ in DRM at 800 °C, giving the highest conversion and good stability of the catalyst.

A stable performance and constant CH_4 and CO_2 conversion were obtained over 15Ni−15Ce−20Al (Table 7). This catalyst and 15Ni−35Ce exhibited the smallest metal particle size after TOS for 30 min among the studied catalysts. The high metal dispersion and a small size of Ni−NPs (15 nm) minimized the coke formation during DRM, maintaining stable catalytic activity for prolonged periods,[68] mostly related to the presence of Ni−CeO_2. Furthermore, the amount of strong basic sites was higher in 15Ni−15Ce−20Al than in 15Ni−15La−20Al, which according to[55], increases catalyst stability. However, despite a stable performance of 15Ni−15Ce−20Al, it accumulated the third-highest amount of carbon deposits per Ni after 30 min of TOS, as confirmed by CHNS (Table 7). Based on XRD, the original phases CeO_2 and Ni^0 remained the same, although the crystallinity of the catalyst was low (Figure 1). It can, however, be observed from Figure 1a that Ni^0 particles are located on the tips of carbon nanofibers and exhibit still activity as reported in[69]. According to[55], CeO_2 can enable Ni-based catalysts to enhance CO_2 activation according to $Ce_2O_3 + CO_2 \rightarrow 2CeO_2 + CO$. In the current case, Ce_2O_3 was not identified in the XRD pattern of the 15Ni−15Ce−20Al catalyst tested in DRM at 850 °C for 30 min of TOS. This phase was, however, formed in the long-term exposure of the catalyst at a high temperature (Figure 1).

The H_2/CO ratio is an important descriptor of DRM, being equal to unity for the stoichiometric reaction. The H_2/CO ratio above unity demonstrates the excess of H_2 production and CH_4 decomposition occurring during DRM for 30 min of TOS. In the current case, the H_2/CO ratio varied in the range of 1.4−1.6, with the lowest one obtained for 15Ni−15La−

https://doi.org/10.1021/acs.iecr.3c02341
Ind. Eng. Chem. Res. 2023, 62, 20588−20607

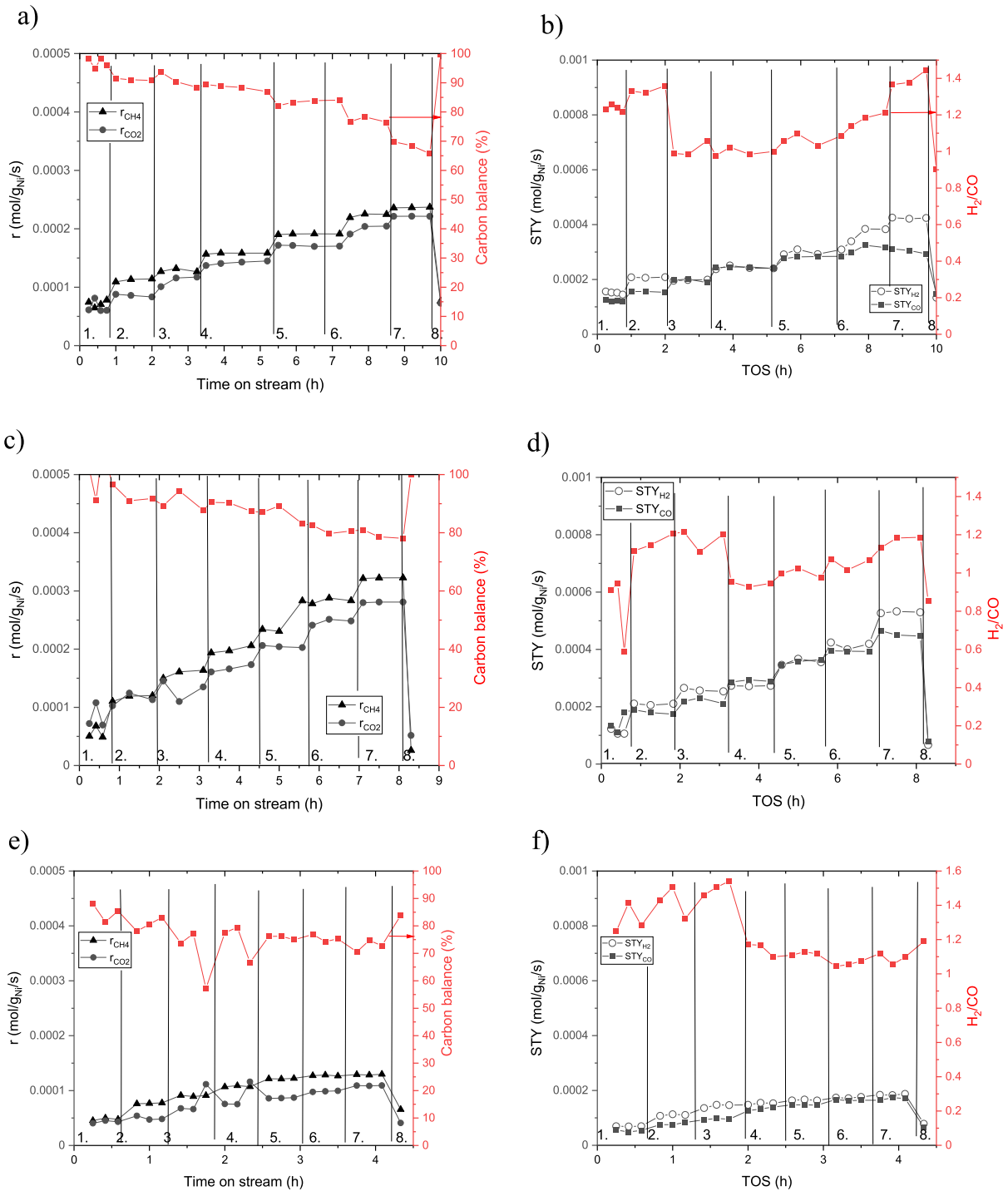

Figure 10. Experimental data on temperature-dependent DRM on nickel alumina catalysts: (a,c) rate for methane and CO_2 transformation and carbon balance and (b,d) space-time yields (STYs) of H_2 and CO and the H_2/CO ratio in dry methane reforming in the temperature range of 600−900 °C and return to 600 °C. Conditions: V_{cat} = 2 mL, GHSV = 3000 h^{-1}, 100 mL/min. Catalysts: (a,b) 15Ni−15Ce−20Al, (c,d) 15Ni−15La−20Al, and (e,f) 15Ni−15Ce−20La. Notation: 1. 600, 2. 650 °C, second day 3. 700, 4. 750, 5. 800, 6. 850, 7. 900, and 8. 600 °C.

20Al, while for, for example, 15Ni−15Ce−20Al, this ratio was 1.5. When comparing the results with the literature,[64] the Ni−Al_2O_3−CeO_2 catalyst prepared by the sol−gel method with a Ni/Ce molar ratio of 3.4 gave a H_2/CO ratio close to unity in DRM at 850 °C, while its counterpart prepared by the impregnation method resulted in a H_2/CO ratio of 0.8. In the current case, 15Ni−15Ce−20Al contained Ni/Ce with a molar ratio of 1.35. Thus, it can be concluded that the catalyst preparation method resulting in close interactions between metals and an optimized Ni/Ce molar ratio has a large impact on DRM.

Effect of Temperature Cycling in DRM over Trimetallic Ni−Al-Based Catalysts. The effect of temperature cycling was studied for both Ni−Ce−Al and Ni−La−Al catalysts by increasing the temperature after 10−15 min of TOS from 600 to 900 °C with a step of 50 °C and returning back to 600 °C (Figure 10). Over the Ni−Ce−Al catalyst, the transformation rate of methane was 21% higher than the CO_2

https://doi.org/10.1021/acs.iecr.3c02341
Ind. Eng. Chem. Res. 2023, 62, 20588−20607

transformation rate at 600 °C. The catalyst retained its activity because the transformation rates of CH_4 and CO_2 were also 21 and 20% at 600 °C at the end of the reaction (Table 8). Although the carbon balance decreased initially from close to 100 to 66 and 78% for Ni−Ce−Al and Ni−La−Al, respectively, at 600 °C, the full carbon balance was recovered.

15Ni−15Ce−20Al exhibited initially at 600 °Ca higher methane transformation activity and a lower CO_2 transformation rate than 15Ni−15La−20Al, while at 800 °C, the activity for both transformations over 15Ni−15Ce−20Al was lower than that for 15Ni−15La−20Al. The initial TOFs for methane transformation decreased for the trimetallic catalysts as follows: 15Ni−15La−20Al > 15Ni−15Ce−20Al > 15Ni−15Ce−20La, which correlated well with the hydrogen consumption in TPR (Table 5).

The space-time yields for H_2 and CO were higher for the 15Ni−15La−20Al catalyst than for 15Ni−15Ce−20Al. Interestingly, the H_2/CO ratio at 800 °C was close to unity, opposite to the results obtained at 850 °C. These results might be due to the formation of $CeAlO_3$ and $LaAlO_3$ (Figure 1), respectively, when the catalysts were treated with a stepwise temperature increase. On the other hand, heating up the 15Ni−15Ce−20Al and 15Ni−15La−20Al catalysts for a short time up to 850 °C did not promote these phase transformations. The activation energies for the methane transformation calculated using the Arrhenius equation were in the range of 36−37 kJ/mol, which are close to the values of 32−56 kJ/mol reported in the literature for Ni-based catalysts.[45,57,70]

According to the literature,[37] the presence of $CeAlO_3$ limits the formation of graphitic carbon; subsequently, the stable performance of 15Ni−15Ce−20Al can be related to the formation of this phase during DRM in the temperature cycling experiments. It was also suggested[40] that $CeAlO_3$ can react with CO_2 during DRM as follows (eq 20)

$$2CeAlO_3 + CO_2 \rightarrow Al_2O_3 + 2CeO_2 + CO \quad (20)$$

Analogously low carbon accumulation was observed in DRM at 800 °C for 10 wt % Ni supported on Ce−AlO[43] with a molar ratio of Ni/Ce equal to 2. During catalyst reduction at 900 °C, the $CeAlO_3$ phase was already formed, while reduction with hydrogen at 800 °C was not enough. Furthermore, when the catalyst reduced at 800 °C was tested in DRM at 800 °C for 18 h, the $CeAlO_3$ phase was formed. In the current case, $CeAlO_3$ was formed during DRM in the temperature cycling experiment as well as in the long-term experiment when the molar ratio of Ni/Ce was 1.35. As a comparison, the rates for methane and CO_2 transformations over 15Ni−15Ce−20La at 600 °C are only 68 and 70% (Figure 10e,f and Table 8), respectively, of those reported for 15Ni−15Ce−20Al. This result correlates well with the low hydrogen consumption determined for 15Ni−15Ce−20La (Table 6). In addition, after DRM in the temperature cycling experiment, large metal particles were observed in TEM images (Table 1 and Figure 2e), showing clearly that the performance of this catalyst was not comparable with the performance at 15Ni−15Ce−20Al, while it was stated in[71] that the La_2O_3−$La_2Ce_2O_7$ mixture is beneficial in DRM, hindering carbon formation; however, in the current case, no La_2O_3 phase was observed.

The H_2/CO ratio for 15Ni−15Ce−20Al varied in the range of 1.0−1.4 with TOS, while for 15Ni−15La−20Al, it was in the range of 0.9−1.2. Formation of the perovskite-type $LaAlO_3$ is thus promising as it can serve as a support for the DRM catalyst, as also reported for Ni of ca. 21 nm size supported on

Table 8. Rates of CH_4 and CO_2 Transformations and the Carbon Balance (CB) at 600 °C Initially and after Temperature Cycling at 600 °C and Rate for CH_4 and CO_2 Transformations at 800 °C over Different Catalysts Calculated from the Experiments with Temperature Cycling from 600 to 900 °C and back to 600 °C[a]

entry	catalyst	$r_{CH_4,600\ °C}$ (mol/s/g_{Ni})	$r_{CO_2,600\ °C}$ (mol/s/g_{Ni})	TOF_{CH_4} (s^{-1})	$CB_{600\ °C}$ (%)	$r_{CH_4,800\ °C}$ (mol/s/g_{Ni})	$r_{CO_2,800\ °C}$ (mol/s/g_{Ni})	$CB_{800\ °C}$ (%)	$STY_{H_2,800\ °C}$ (mol/s/g_{Ni})	$STY_{CO,800\ °C}$ (mol/s/g_{Ni})	H_2/CO	E_A (kJ/mol)
1	15Ni−15Ce−20Al	7.4×10^{-5} (7.6×10^{-5})	6.1×10^{-5} (7.3×10^{-5})	0.08	98 (99)	1.9×10^{-4}	1.7×10^{-4}	82	2.9×10^{-4}	2.8×10^{-4}	1.0	38 (600−750 °C) 23 (800−900 °C)
2	15Ni−15Ce−15La	$4.8 \times 10-5$ (4.1×10^{-5})	4.3×10^{-5} (4.1×10^{-5})	0.07	85 (84)	1.2×10^{-4}	0.87×10^{-4}	75	1.6×10^{-4}	1.5×10^{-4}	1.1	39 (600−750 °C) 6 (800−900 °C)
3	15Ni−15La−20Al	5.0×10^{-5} (2.6×10^{-5})	7.2×10^{-5} (5.2×10^{-5})	0.1	100 (100)	2.3×10^{-5}	2.1×10^{-5}	87	3.5×10^{-4}	3.5×10^{-4}	1.0	62 (600−750 °C) 27 (800−900 °C)

[a]In parentheses, the final conversion at 600 °C is given.

https://doi.org/10.1021/acs.iecr.3c02341
Ind. Eng. Chem. Res. 2023, 62, 20588−20607

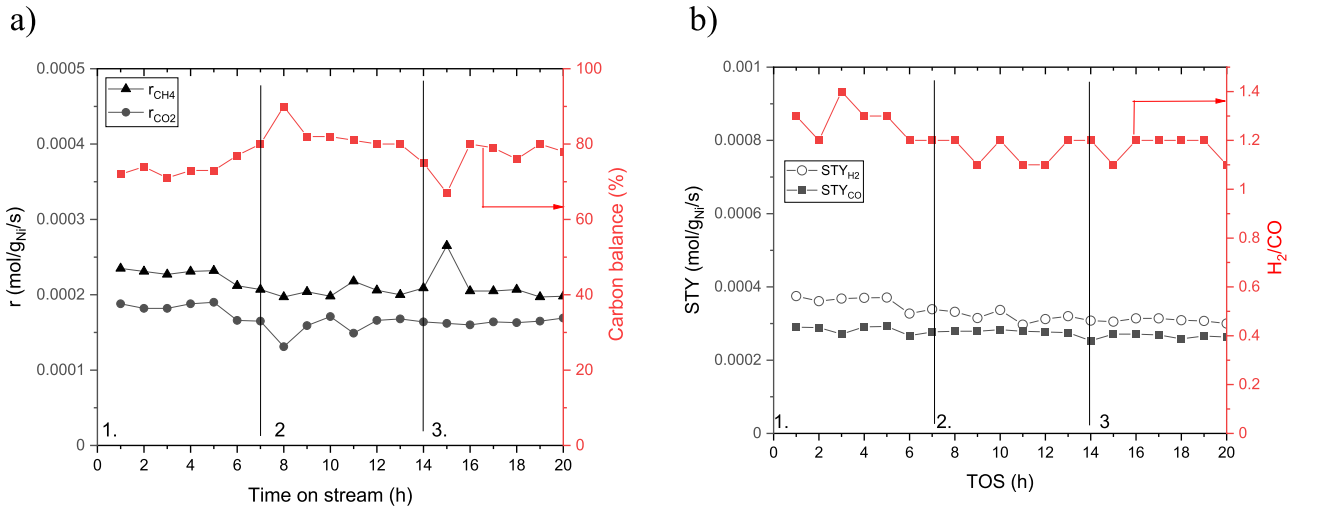

Figure 11. Long-term TOS performance of 15Ni−15Ce−20Al at 850 °C, (a) transformation rates for methane and CO_2 and carbon balance, and (b) space-time yields of CO and H_2 and the H_2/CO ratio. Conditions: V_{cat} = 2 mL, GHSV = 3000 h^{-1}, 100 mL/min. Notation: 1. first experiment was performed for 7 h of TOS, followed by two more days with TOSs of 7 h (second day) and 6 h (third day).

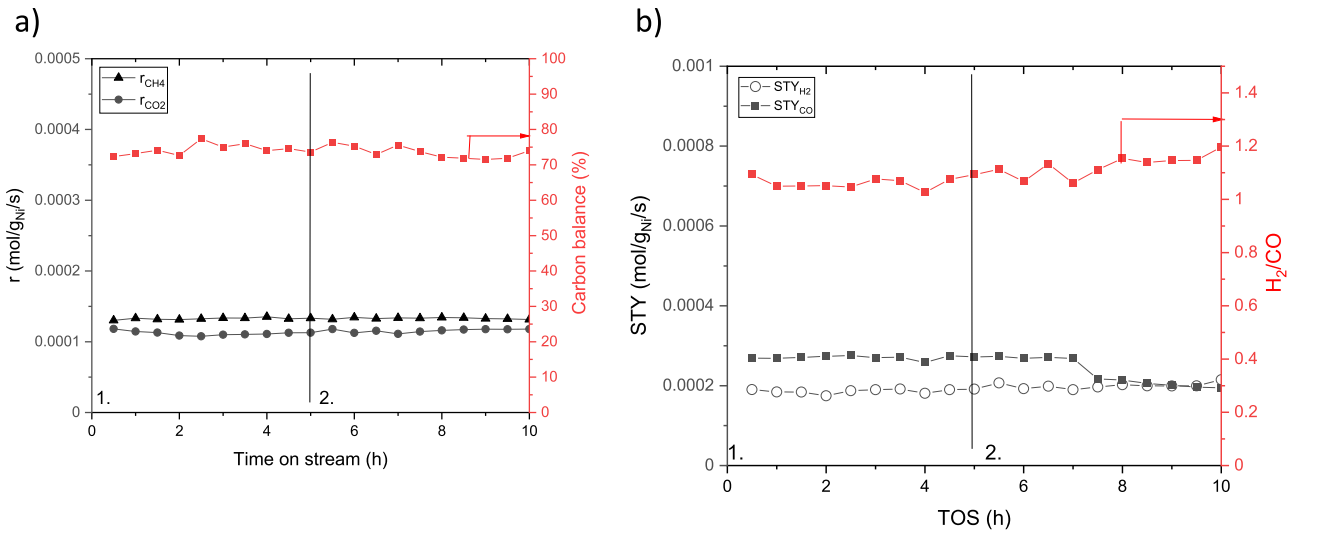

Figure 12. Long-term TOS performance of 12Ni−α-Al_2O_3 at 850 °C, (a) transformation rates for methane and CO_2 and carbon balance, and (b) space-time yields of CO and H_2 and the H_2/CO ratio. Conditions: V_{cat} = 2 mL, GHSV = 3000 h^{-1}, 100 mL/min. Notation: 1. first experiment was performed for 5 h of TOS, followed by two more days with a TOS of 5 h (second day).

ceria and lantana alumina catalysts.[42] It is reported in ref 72 that the H_2/CO ratio was ca. 1.2 over Ni/$LaAlO_3$ during DRM at 700 °C using a GHSV of 18 L/(g·h) at a TOS of 10 h. This H_2/CO value is the same as in the current case over 15Ni−15La−20Al at 700 °C. Thermodynamic analysis in ref 73 gave a H_2/CO ratio of ca. 1.1 at 800 °C, close to those obtained in the current work. The H_2/CO ratio's decrease to 0.8 at the end of the experiment at 600 °C is due to a higher CO_2 conversion at 900 °C in comparison to CH_4 conversion. Higher CO_2 conversion indicates the RWGS reaction to occur, which consumes more hydrogen, yielding a lower H_2/CO ratio as a consequence. The equilibrium H_2/CO ratio at 600 °C is ca. 3.[60]

Long-Time Stability. Due to the relatively better performance of the 15Ni−15Ce−20Al catalyst, its long-term stability was further elucidated at 850 °C using a GHSV of 3000 h^{-1} for a longer time of 7 h and continuing the experiment on the next day for 7 h and onto the third day for 6 h with the same catalyst. The results showed that the methane transformation rate was ca. 40% higher than that for CO_2, being stable for 14 h (Figure 11a). At the same time, the carbon balance was ca. 75%. The H_2/CO ratio varied in the range of 1.0−1.2, which is very good.

Furthermore, when comparing the carbon accumulation rate determined from CHNS analysis for 15Ni−15Ce−20Al catalysts for TOSs of 0.5 and 20 h, respectively, the rates were 13.8 and 1.3 wt %/h, indicating that carbon accumulation was initially more than 10-fold higher than with a longer TOS. This result is explained by adsorption of filamentous coke, which is deposited both on the metal and acidic sites, being available at the beginning of the reaction. The temperature of filamentous coke formation was discussed in conjunction with TGA.[74]

As a comparison, the performance of Ni/α-Al_2O_3 remained stable for 10 h of TOS (Figure 12). The deactivation rate calculated from methane transformation was zero for both Ni/α-Al_2O_3 and 15Ni−15Ce−20Al during 10 h of TOS (Table 9), while for 20 h of TOS, it was 0.04%/min. The higher

https://doi.org/10.1021/acs.iecr.3c02341
Ind. Eng. Chem. Res. 2023, 62, 20588−20607

Table 9. Results from Long-Term Stability Tests of Ni−Ce−Al Catalysts in DRM at 850 °C[a]

entry	catalyst	T = 850 °C, V_{cat} = 2 mL, GHSV = 3000 h^{-1}, 100 mL/min, 20 h TOS	$r_{CH_4,0}$ (mol/s/g_{Ni})	$r_{CO_2,600\ °C}$ (mol/s/g_{Ni})	$CB_{600\ °C}$ (%)	STY_{H_2} (mol/s/g_{Ni})	STY_{CO_2} (mol/s/g_{Ni})	H_2/CO	deactivation in X_{CH_4}%/min	references
1	15Ni−15Ce−20Al	T = 850 °C, V_{cat} = 2 mL, GHSV = 3000 h^{-1}, 100 mL/min, 20 h TOS	2.4 × 10^{-4} (1.9 × 10^{-4})	1.9 × 10^{-4} (1.7 × 10^{-4})	72 (78)	3.8 × 10^{-4} (3.0 × 10^{-4})	2.9 × 10^{-4} (2.6 × 10^{-4})	1.3	0	this work
2	12 wt % Ni/α-Al_2O_3	T = 850 °C, V_{cat} = 2 mL, GHSV = 3000 h^{-1}, 100 mL/min, 10 h TOS	[b]1.3 × 10^{-4} (1.3 × 10^{-4})	[b]1.2 × 10^{-4} (1.2 × 10^{-4})	[b]72 (74)	[b]1.9 × 10^{-4} (2.1 × 10^{-4})	[b]2.7 × 10^{-4} (1.9 × 10^{-4})	[b]1.2	0	this work
3	9.4 wt % Ni−10 wt % Ce−Al	T = 800 °C, GHSV = 90,000 cm^3/(g h), 20 h TOS	n.d	n.d	n.d	n.d	n.d	0.88	0	37

[a]Notation: $r_{CH_4,0}$ and $r_{CO_2,0}$ are the initial transformation rates of methane and CO_2, respectively, while the corresponding values in parentheses are after 20 h of TOS. [b]The initial transformation rates of methane and CO_2 and, in parenthesis, the values after 10 h of TOS.

deactivation rate observed after 10 h of TOS in the long-term experiment can be due to partial transformation of $CeAlO_3$ to CeO_2, as suggested by the potential CeO_2 phase observed in the XRD (Figure 2). This phase is formed in a reducing atmosphere at high temperature when CeO_2 reacts with Al_2O_3 to form the $CeAlO_3$ phase, according to eqs 17 and 18. It was also stated in ref 37 that $CeAlO_3$ could react with CO_2 to form CO and CeO_2 (eq 20), and thereafter, CeO_2 can oxidize the CH_x species located at the Ni-support boundary, restoring the $CeAlO_3$ sites (eq 21)

$$Al_2O_3 + 2CeO_2 + CH_x \rightarrow CO + 2CeAlO_3 + (x/2)H_2 \quad (21)$$

In the current case, no CeO_2 phase was observed in the spent catalyst after 10 h of TOS, while after 10 h of TOS, the $CeAlO_3$ phase appears to be partially oxidized to CeO_2 (eq 22). It was also stated that methane decomposition occurring on active metal sites is followed by a reaction with the surface CO_2 species or the adsorbed oxygen atoms derived from CO_2 is involved in one of them

$$CO_2 + * \rightarrow CO + O^* \quad (22)$$

where * denotes a metallic nickel active site or an oxygen vacancy over ceria, while O* means adsorbed oxygen species over nickel or an occupied oxygen vacancy.[42]

The deactivation rate for Ni−Ce−Al reported in the literature[37] was of an analogous extent, although the corresponding experiment was performed at 750 °C. Thus, it can be concluded that performance of 15Ni−15Ce−20Al was comparable to that of Ni/α-Al_2O_3 for 10 h of TOS at 850 °C in DRM.

The long-term stability of 15Ni−15Ce−20Al was compared with the performance of 12 wt % Ni/α-Al_2O_3 (Table 9). The results showed that the methane transformation rate was 1.3 and 1.1-fold higher than the CO transformation rate for 15Ni−15Ce−20Al and 12 wt % Ni/α-Al_2O_3, respectively. Furthermore, the performance of the trimetallic catalyst was better than that obtained for 12 wt % Ni/α-Al_2O_3, that is, the methane transformation rate for the former catalyst was 1.8-fold that for 12 wt % Ni/α-Al_2O_3. When STY yields calculated per mass of Ni were compared, the trimetallic catalyst was also more active. The H_2/CO ratio was slightly higher for the trimetallic catalyst compared to that for 12 wt % Ni/α-Al_2O_3. Both catalysts, however, remained stable during the DRM and no deactivation calculated from the methane transformation rate was observed despite coking. As a comparison with the literature,[37] DRM was performed over 9 wt % Ni−Ce−Al_2O_3 catalyst with a Ni/Ce molar ratio of 1.5 prepared by the coprecipitation method. The space-time yield of hydrogen at 800 °C was 16 s^{-1} calculated per mole of active nickel on the surface. Also noteworthy is the fact that Ni−Ce−Al_2O_3 gave a H_2/CO ratio of 0.88, which differs from the current results. It was, however, pointed out in ref 37 that the reverse water gas shift reaction is more prominent at the lower temperature range of 700−850 °C and the highest reaction temperature in ref 31 was 800 °C, while in the current case, it was 850 °C.

As shown in Table 10, the performance of 15Ni−15Ce−20Al was compared with other catalysts reported in the literature, showing conversion and initial turnover frequencies calculated as moles of methane reacted per moles of exposed Ni surface divided by time. The conversion levels over 15Ni−15Ce−20Al for methane and CO_2 were 45 and 70% of those obtained for 12.2 wt % Ni−α-Al_2O_3 (Table 10). It should,

https://doi.org/10.1021/acs.iecr.3c02341
Ind. Eng. Chem. Res. 2023, 62, 20588−20607

Table 10. Comparison of TOFs Calculated from Methane Transformation per Moles of Exposed Surface of Nickel

catalyst	conditions	TOF (s^{-1})	X_{CH_4} (%)	X_{CO_2} (%)	deactivation in X_{CH_4}%/min	references
15Ni−15Ce−20Al	T = 850 °C, V_{cat} = 2 mL, GHSV = 3000 h^{-1}, 100 mL/min, 15,957 mL/(h g_{cat}), 20 h TOS	0.31	43	65	0.04	this work
12 wt % Ni/α-Al_2O_3	T = 850 °C, V_{cat} = 2 mL, GHSV = 3000 h^{-1}, 4511 mL/(h g_{cat}), 100 mL/min, 10 h TOS	0.10	94	90	0	this work
Ni−Ce−Al	T = 800 °C, m_{cat} = 100 mg, GHSV = 36,000 mL/(h g_{cat}), 80 h TOS	1.15	91	80	very low	76
10Ni−1Al−1Ce	T = 700 °C, m_{cat} = 100 mg, GHSV = 120,000 mL/(h g_{cat}), 200 mL/min, 8 h TOS	4.0	82	91	n.d	77
Ni−α-Al_2O_3	T = 800 °C, m_{cat} = 100 mg, GHSV = 50,000 mL/(h g_{cat}), 100 h TOS	81.2	86	91	0.05	75

however, be kept in mind that the catalyst volume was the same in these experiments, but masses varied. The higher conversion was obtained over 12.2 wt % Ni−α-Al_2O_3, for which the conversion levels were nearly the same as those obtained at thermodynamic equilibrium (Figure 7). Methane conversion at thermodynamic equilibrium at 850 °C is ca. 98%, while that at CO_2 is slightly lower, being ca. 90%.

Furthermore, TOFs which take into account exposed surface moles of nickel were close to the results obtained in[75,76], which demonstrated a high performance of catalysts in DRM. In the current case, relatively large metal particle sizes varying between 12 and 23 nm (Table 1) were observed, most probably due to low specific surface areas of the catalysts prepared by the solution combustion method. However, TOFs are still in the same order of magnitude as reported earlier.[76,77] On the other hand, TOF values calculated in ref 77 were much higher than that of other catalysts demonstrated in Table 10. Overall, it can be stated that the obtained results were comparable to those obtained with 12 wt % Ni/α-Al_2O_3, which is important from a practical point of view for industrial application.

CONCLUSIONS

Several bi- and trimetallic Ce−Al oxide catalysts were prepared by the solution combustion method, characterized by various physicochemical methods, and tested in DRM. The surface areas of the prepared catalyst were in the range of 3−12 m^2/g, which is typical for this type of catalyst. The metal particle sizes varied between 12 and 26 nm, and the largest metal particle sizes of the spent catalysts were observed for the Ni−Ce−La catalyst, indicating that the presence of Al can suppress sintering. The most acidic catalyst was the monometallic reference catalyst Ni−α-Al_2O_3, with a large aluminum content, while lower acidities were observed for trimetallic Ni−Ce−Al and Ni−La−Al catalysts. On the other hand, the most basic catalyst was Ni−La, while very low basicity was recorded for the trimetallic counterparts Ni−Ce−Al and Ni−La−Al. XRD results of the fresh and spent catalysts revealed that bimetallic Ni−La and Ni−Ce catalysts exhibited low crystallinity analogously to the fresh trimetallic catalysts. On the other hand, the crystallinity of the trimetallic catalysts increased with the increase in the severity during DRM, and at the same time, metallic Ni appeared during DRM. $CeAlO_3$ and $LaAlO_3$ phases were formed during DRM in Ni−Ce−Al and Ni−La−Al catalysts, respectively, which might facilitate better stability of the catalyst.

In the preliminary catalyst testing, short-term tests with 30 min TOS at 850 °C were performed, and methane transformation was observed to be structure-sensitive. The highest methane transformation rate also promoted the highest catalyst deactivation rate. Based on the initial catalyst screening, temperature stability for trimetallic Ni−Ce−Al, Ni−La−Al, and Ni−Ce−La was investigated via cycling the temperature during DRM from 600 to 700 to 800 to 900 °C and back to 600 °C. The results showed that the most stable performance was observed for Ni−Ce−Al, while both Ni−Ce−La and Ni−La−Al gave lower methane transformation rates when returning the temperature back to 600 °C. For all these catalysts, the H_2/CO ratio was, however, close to 1.0−1.1.

Long-term stability tests for Ni−Ce−Al and Ni−α-Al_2O_3 catalysts showed that the former catalyst exhibited 3.1-fold higher TOF than the latter reference catalyst, and no measurable deactivation was observed during long-term tests for both catalysts. TOF values were also in the same order of magnitude as compared with literature data, indicating that the solution combustion method is a promising alternative for DRM reaction.

ASSOCIATED CONTENT

Supporting Information

The Supporting Information is available free of charge at https://pubs.acs.org/doi/10.1021/acs.iecr.3c02341.

XRD patterns of reduced catalysts, overview of the catalytic results over supported alkali metal-modified nickel catalysts, and elemental analysis of the catalysts (PDF)

AUTHOR INFORMATION

Corresponding Authors

Alua Manabayeva − *Kazakh-British Technical University, Almaty, KZ 050000, Kazakhstan; Laboratory of Industrial Chemistry and Reaction Engineering, Åbo Akademi University, Turku/Åbo 20500, Finland; D.V. Sokolsky Institute of Fuel, Catalysis and Electrochemistry, Almaty, KZ 050010, Kazakhstan*; Email: manabaeva_2018@mail.ru

Dmitry Yu. Murzin − *Laboratory of Industrial Chemistry and Reaction Engineering, Åbo Akademi University, Turku/Åbo 20500, Finland; D.V. Sokolsky Institute of Fuel, Catalysis and Electrochemistry, Almaty, KZ 050010, Kazakhstan*; orcid.org/0000-0003-0788-2643; Email: dmitry.murzin@abo.fi

Authors

Päivi Mäki-Arvela − *Laboratory of Industrial Chemistry and Reaction Engineering, Åbo Akademi University, Turku/Åbo 20500, Finland*; orcid.org/0000-0002-7055-9358

Zuzana Vajglová − *Laboratory of Industrial Chemistry and Reaction Engineering, Åbo Akademi University, Turku/Åbo 20500, Finland*

Mark Martinez-Klimov − *Laboratory of Industrial Chemistry and Reaction Engineering, Åbo Akademi University, Turku/Åbo 20500, Finland*

https://doi.org/10.1021/acs.iecr.3c02341
Ind. Eng. Chem. Res. 2023, 62, 20588−20607

Olha Yevdokimova − *Laboratory of Industrial Chemistry and Reaction Engineering, Åbo Akademi University, Turku/Åbo 20500, Finland*
Anssi Peuronen − *Department of Chemistry, University of Turku, Turku, FI 20014, Finland*
Mika Lastusaari − *Department of Chemistry, University of Turku, Turku, FI 20014, Finland;* orcid.org/0000-0003-1872-0391
Teija Tirri − *Laboratory of Industrial Chemistry and Reaction Engineering, Åbo Akademi University, Turku/Åbo 20500, Finland*
Kaisar Kassymkan − *D.V. Sokolsky Institute of Fuel, Catalysis and Electrochemistry, Almaty, KZ 050010, Kazakhstan*
Tolkyn S. Baizhumanova − *D.V. Sokolsky Institute of Fuel, Catalysis and Electrochemistry, Almaty, KZ 050010, Kazakhstan; Al-Farabi Kazakh National University, Almaty, KZ 050040, Kazakhstan*
Manapkhan Zhumabek − *D.V. Sokolsky Institute of Fuel, Catalysis and Electrochemistry, Almaty, KZ 050010, Kazakhstan*
Rabiga O. Sarsenova − *D.V. Sokolsky Institute of Fuel, Catalysis and Electrochemistry, Almaty, KZ 050010, Kazakhstan*
Zauresh T. Zheksenbaeva − *D.V. Sokolsky Institute of Fuel, Catalysis and Electrochemistry, Almaty, KZ 050010, Kazakhstan*
Gulnar N. Kaumenova − *D.V. Sokolsky Institute of Fuel, Catalysis and Electrochemistry, Almaty, KZ 050010, Kazakhstan*
Vincenzo Russo − *Università di Napoli Federico II, Napoli, IT 80126, Italy;* orcid.org/0000-0002-1867-739X
Svetlana A. Tungatarova − *D.V. Sokolsky Institute of Fuel, Catalysis and Electrochemistry, Almaty, KZ 050010, Kazakhstan; Al-Farabi Kazakh National University, Almaty, KZ 050040, Kazakhstan*

Complete contact information is available at: https://pubs.acs.org/10.1021/acs.iecr.3c02341

Notes

The authors declare no competing financial interest.

■ ACKNOWLEDGMENTS

This research has been funded by the Science Committee of the Ministry of Education and Science of the Republic of Kazakhstan (grant no. AP14869966).

■ LIST OF SYMBOLS

T temperature, °C
x_i molar fraction of component i, -

■ REFERENCES

(1) Mosinska, M.; Szynkowska, M. I.; Mierczynski, P. Oxy-steam reforming of natural gas on Ni catalysts—A minireview. *Catalysts* **2020**, *10* (8), 896−923.
(2) Chong, C. C.; Cheng, Y. W.; Bukhari, S. N.; Setiabudi, H. D.; Jalil, A. A. Methane dry reforming over Ni/fibrous SBA-15 catalysts: Effects of support morphology (rod-liked F-SBA-15 and dendritic DFSBA-15). *Catal. Today* **2021**, *375*, 245−257.
(3) Goula, M. A.; Charisiou, N. D.; Siakavelas, G.; Tzounis, L.; Tsiaoussis, I.; Panagiotopoulou, P.; Goula, G.; Yentekakis, I. V. Syngas production via the biogas dry reforming reaction over Ni supported on zirconia modified with CeO_2 or La_2O_3 catalysts. *Int. J. Hydrogen Energy* **2017**, *42* (19), 13724−13740.
(4) Ekeoma, B. C.; Yusuf, M.; Johari, K.; Abdullah, B. Mesoporous silica supported Ni-based catalysts for methane dry reforming: A review of recent studies. *Int. J. Hydrogen Energy* **2022**, *47* (98), 41596−41620.
(5) Karemore, A. L.; Sinha, R.; Chugh, P.; Vaidya, P. D. Syngas production by carbon dioxide reforming of methane over Pt/Al_2O_3 and Pt/ZrO_2-SiO_2 catalysts. *Chem. Eng. Sci.* **2022**, *249*, 117347.
(6) Jin, B.; Li, S.; Liang, X. Enhanced activity and stability of MgO-promoted Ni/Al_2O_3 catalyst for dry reforming of methane: Role of MgO. *Fuel* **2021**, *284*, 119082−119092.
(7) Georgiadis, A. G.; Siakavelas, G. I.; Tsiotsias, A. I.; Charisiou, N. D.; Ehrhardt, B.; Wang, W.; Sebastian, V.; Hinder, S. J.; Baker, M. A.; Mascotto, S.; Goula, M. A. Biogas dry reforming over Ni/LnO_x-type catalysts (Ln = La, Ce, Sm or Pr). *Int. J. Hydrogen Energy* **2023**, *48*, 19953−19971.
(8) Bakhtiari, K.; Shahbazi Kootenaei, A.; Maghsoodi, S.; Azizi, S.; Tabatabaei Ghomsheh, S. M. Synthesis of high sintering-resistant Ni-modified halloysite based catalysts containing La, Ce, and Co for dry reforming of methane. *Ceram. Int.* **2022**, *48* (24), 37394−37402.
(9) Loc, L. C.; Phuong, P. H.; Tri, N. Role of CeO_2 promoter in NiO/α-Al_2O_3 catalyst for dry reforming of methane. *AIP Conf. Proceed.* **2017**, *1878*, 020033.
(10) Sepehri, S.; Rezaei, M. Ce promoting effect on the activity and coke formation of Ni catalysts supported on mesoporous nanocrystalline γ-Al_2O_3 in autothermal reforming of methane. *Int. J. Hydrogen Energy* **2017**, *42*, 11130−11138.
(11) Xu, S.; Slater, T. J. A.; Huang, H.; Zhou, Y.; Jiao, Y.; Parlett, C. M. A.; Guan, S.; Chansai, S.; Xu, S.; Wang, X.; Hardacre, C.; Fan, X. Developing silicalite-1 encapsulated Ni nanoparticles as sintering-/coking-resistant catalysts for dry reforming of methane. *Chem. Eng. J.* **2022**, *446*, 137439−137452.
(12) Gao, X.; Ge, Z.; Zhu, G.; Wang, Z.; Ashok, J.; Kawi, S. Anti-coking and anti-sintering Ni/Al_2O_3 catalysts in the dry reforming of methane: Recent progress and prospects. *Catalysts* **2021**, *11*, 1003−1023.
(13) Kim, S. B.; Eissa, A. A.-S.; Kim, M.-J.; Goda, E. S.; Youn, J.-R.; Lee, K. Sustainable synthesis of a highly stable and coke-free Ni@CeO_2 catalyst for the efficient carbon dioxide reforming of methane. *Catalysts* **2022**, *12*, 423−446.
(14) Chein, R.-Y.; Fung, W.-Y. Syngas production via dry reforming of methane over CeO_2 modified Ni/Al_2O_3 catalysts. *Int. J. Hydrogen Energy* **2019**, *44*, 14303−14315.
(15) Zhang, Y.; Zeng, R.; Zu, Y.; Zhu, L.; Mei, Y.; Luo, Y.; He, D. Low-temperature dry reforming of methane tuned by chemical speciations of active sites on the SiO_2 and γ-Al_2O_3 supported Ni and Ni-Ce catalysts. *Chin. J. Chem. Eng.* **2022**, *48*, 76−90.
(16) Marinho, A. L. A.; Toniolo, F. S.; Noronha, F. B.; Epron, F.; Duprez, D.; Bion, N. Highly active and stable Ni dispersed on mesoporous CeO_2-Al_2O_3 catalysts for production of syngas by dry reforming of methane. *Appl. Catal., B* **2021**, *281*, 119459.
(17) Du, X.; Zhang, D.; Shi, L.; Gao, R.; Zhang, J. Morphology dependence of catalytic properties of Ni/CeO_2 nanostructures for carbon dioxide reforming of methane. *J. Phys. Chem. C* **2012**, *116* (18), 10009−10016.
(18) Bian, Z.; Zhong, W.; Yu, Y.; Wang, Z.; Jiang, B.; Kawi, S. Dry reforming of methane on Ni/mesoporous-Al_2O_3 catalysts: Effect of calcination temperature. *Int. J. Hydrogen Energy* **2021**, *46* (60), 31041−31053.
(19) Al-Fatesh, A. S.; Naeem, M. A.; Fakeeha, A. H.; Abasaeed, A. E. Role of La_2O_3 as promoter and support in Ni/γ-Al_2O_3 catalysts for dry reforming of methane. *Chin. J. Chem. Eng.* **2014**, *22* (1), 28−37.
(20) Manabayeva, A. M.; Mäki-Arvela, P.; Vajglová, Z.; Martinez-Klimov, M.; Tirri, T.; Baizhumanova, T. S.; Grigor'eva, V. P.; Zhumabek, M.; Aubakirov, Y. A.; Simakova, I.; Murzin, D.; Tungatarova, S. A. Dry reforming of methane over Ni-Fe-Al catalysts prepared by solution combustion synthesis. *Ind. Eng. Chem. Res.* **2023**, *62* (29), 11439−11455.

(21) Martínez, R.; Romero, E.; Guimon, C.; Bilbao, R. CO_2 reforming of methane over coprecipitated Ni-Al catalysts modified with lanthanum. *Appl. Catal., A* **2004**, *274*, 139−149.
(22) Tsiotsias, A. I.; Charisiou, N. D.; Sebastian, V.; Gaber, S.; Hinder, S. J.; Baker, M. A.; Polychronopoulou, K.; Goula, M. A. A comparative study of Ni catalysts supported on Al_2O_3, MgO-CaO-Al_2O_3 and La_2O_3- Al_2O_3 for the dry reforming of ethane. *Int. J. Hydrogen Energy* **2022**, *47*, 5337−5353.
(23) Georgiadis, A. G.; Siakavelas, G. I.; Tsiotsias, A. I.; Charisiou, N. D.; Ehrhardt, B.; Wang, W.; Sebastian, V.; Hinder, S. J.; Baker, M. A.; Mascotto, S.; Goula, M. A. Biogas dry reforming over Ni/LnO_x-type catalysts (Ln = La, Ce, Sm or Pr). *Int. J. Hydrogen Energy* **2023**, *48*, 19953−19971.
(24) Novitskaya, E.; Kelly, J. P.; Bhaduri, S.; Graeve, O. A. A review of solution combustion synthesis: an analysis of parameters controlling powder characteristics. *Int. Mater. Rev.* **2021**, *66* (3), 188−214.
(25) Zhumabek, M.; Kaumenova, G.; Augaliev, D.; Alaidar, Y.; Murzin, D.; Tungatarova, S.; Xanthopoulou, G.; Kotov, S.; Baizhumanova, T. Selective catalytic reforming of methane into synthesis gas. *Chem. Eng. Technol.* **2021**, *44* (11), 2026−2033.
(26) Ali, S.; Khader, M. M.; Almarri, M. J.; Abdelmoneim, A. G. Ni-based nano-catalysts for the dry reforming of methane. *Catal. Today* **2020**, *343*, 26−37.
(27) Xanthopoulou, G.; Thoda, O.; Metaxa, E. D.; Vekinis, G.; Chroneos, A. Influence of atomic structure on the nano-nickel-based catalyst activity produced by solution combustion synthesis in the hydrogenation of maleic acid. *J. Catal.* **2017**, *348*, 9−21.
(28) Varma, A.; Mukasyan, A. S.; Rogachev, A. S.; Manukyan, K. V. Solution combustion synthesis of nanoscale materials. *Chem. Rev.* **2016**, *116*, 14493−14586.
(29) He, L.; Hu, S.; Yin, X.; Xu, J.; Han, H.; Li, H.; Ren, Q.; Su, S.; Wang, Y.; Xiang, J. Promoting effects of Fe-Ni alloy on co-production of H_2 and carbon nanotubes during steam reforming of biomass tar over Ni-Fe/α-Al_2O_3. *Fuel* **2020**, *276*, 118116−118124.
(30) Olivares, A. C. V.; Gomez, M. F.; Barroso, M. N.; Abello, M. C. Ni-supported catalysts for ethanol steam reforming: effect of the solvent and metallic precursor in catalyst preparation. *Int. J. Ind. Chem.* **2018**, *9*, 61−73.
(31) Chein, R.-Y.; Chen, Y.-C.; Chen, W.-H. Experimental study on sulfur deactivation and regeneration of ni-based catalyst in dry reforming of biogas. *Catalysts* **2021**, *11*, 777−792.
(32) Ferrandon, M. S.; Byron, C.; Celik, G.; Zhang, Y.; Ni, C.; Sloppy, J.; McCormick, R. A.; Booksh, K.; Teplyakov, A. V.; Delferro, M. Grafted nickel-promoter catalysts for dry reforming of methane identified through high-throughput experimentation. *Appl. Catal., A* **2022**, *629*, 118379−118393.
(33) Murzin, D. Y. *Chemical Reaction Technology*, 2nd ed.; De Gruyter: Berlin, 2022.
(34) ChemCAD v.8. http://www.chemstations.com (accessed Oct 27, 2023).
(35) le Saché, E.; Reina, T. R. Analysis of dry reforming as direct route for gas phase CO_2 conversion. The past, the present and future of catalytic DRM technologies. *Prog. Energy Combust. Sci.* **2022**, *89*, 100970.
(36) Jović, V. D.; Maksimović, V.; Pavlović, M. G.; Popov, I. Morphology, internal structure and growth mechanism of electro-deposited Ni and Co powders. *J. Solid State Electrochem.* **2006**, *10*, 373−379.
(37) Luisetto, I.; Tuti, S.; Battocchio, C.; Lo Mastro, S.; Sodo, A. Ni/CeO_2-Al_2O_3 catalysts for the dry reforming of methane: The effect of $CeAlO_3$ content and nickel crystallite size on catalytic activity and coke resistance. *Appl. Catal., A* **2015**, *500*, 12−22.
(38) Tang, G.; Gong, D.; Liu, H.; Wang, L. Highly loaded mesoporous Ni-La_2O_3 catalyst prepared by colloidal solution combustion method for CO_2 methanation. *Catalysts* **2019**, *9* (5), 442−453.
(39) Gates-Rector, S.; Blanton, T. The powder diffraction file: a quality materials characterization database. *Powder Diffr.* **2019**, *34* (4), 352−360.
(40) Chen, W.; Zhao, G.; Xue, Q.; Chen, L.; Lu, Y. High carbon-resistance Ni/$CeAlO_3$-Al_2O_3 catalyst for CH_4/CO_2 reforming. *Appl. Catal., B* **2013**, *136*−*137*, 260−268.
(41) Kim, T. Y.; Kim, S. M.; Lee, W. S.; Woo, S. I. Effect and behavior of cerium oxide in Ni/γ-Al_2O_3 catalysts on autothermal reforming of methane: $CeAlO_3$ formation and its role on activity. *Int. J. Hydrogen Energy* **2013**, *38* (14), 6027−6032.
(42) Charisiou, N. D.; Siakavelas, G.; Papageridis, K. N.; Baklavaridis, A.; Tzounis, L.; Avraam, D. G.; Goula, M. A. Syngas production via the biogas dry reforming reaction over nickel supported on modified with CeO_2 and/or La_2O_3 alumina catalysts. *J. Nat. Gas Sci. Eng.* **2016**, *31*, 164−183.
(43) Fleming, P.; Farrell, R. A.; Holmes, J. D.; Morris, M. A. The rapid formation of $La(OH)_3$ from La_2O_3 powders on exposure to water vapor. *J. Am. Ceram. Soc.* **2010**, *93* (4), 1187−1194.
(44) Zhou, X.; Vovk, E. I.; Liu, Y.; Guan, C.; Yang, Y. An in-situ temperature-dependent study of La_2O_3 reactivation process. *Front. Chem.* **2021**, *9*, 694559.
(45) Moradi, P.; Parvari, M. Preparation of lanthanum-nickel-aluminium perovskite systems and their application in methane-reforming reactions. *Iran. J. Chem. Eng.* **2006**, *3* (3), 29−43.
(46) Tseng, K.-P. Chemical selection rules of single-phase high-entropy oxides. Doctoral Thesis, University of Illinois at Urbana-Champaign, Urbana, IL, 2020; p 200.
(47) Butt, T. M.; Janjua, N. K.; Mujtaba, A.; Zaman, S. A.; Ansir, R.; Rafique, A.; Sumreen, P.; Mukhtar, M.; Pervaiz, M.; Yaqub, A.; Akhter, Z.; Yasin, T.; Abbas, G.; Raza, R.; Medvedev, D. B-Site doping in lanthanum cerate nanomaterials for water electrocatalysis. *J. Electrochem. Soc.* **2020**, *167* (2), 026503−026513.
(48) Zhang, F. X.; Tracy, C. L.; Lang, M.; Ewing, R. C. Stability of fluorite-type $La_2Ce_2O_7$ under extreme conditions. *J. Alloys Compd.* **2016**, *674*, 168−173.
(49) Liu, Y.; Gao, J.; Liu, Q.; Gu, F.; Lu, X.; Jia, L.; Xu, G.; Zhong, Z.; Su, F. Preparation of high-surface-area Ni/α-Al_2O_3 catalysts for improved CO methanation. *RSC Adv.* **2015**, *5* (10), 7539−7546.
(50) Littlewood, P.; Liu, S.; Weitz, E.; Marks, T. J.; Stair, P. C. Ni-Alumina dry reforming catalysts: Atomic layer deposition and the issue of Ni aluminate. *Catal. Today* **2020**, *343*, 18−25.
(51) Al-Mubaddel, F. S.; Kumar, R.; Sofiu, M. L.; Frusteri, F.; Ibrahim, A. A.; Srivastava, V. K.; Kasim, S. O.; Fakeeha, A. H.; Abasaeed, A. E.; Osman, A. I.; Al-Fatesh, A. S. Optimizing acido-basic profile of support in Ni supported La_2O_3+Al_2O_3 catalyst for dry reforming of methane. *Int. J. Hydrogen Energy* **2021**, *46*, 14225−14235.
(52) Chen, J.; Wang, R.; Zhang, J.; He, F.; Han, S. Effects of preparation methods on properties of Ni/CeO_2-Al_2O_3 catalysts for methane reforming with carbon dioxide. *J. Mol. Catal.* **2005**, *235* (1−2), 302−310.
(53) Kim, S. M.; Armutlulu, A.; Liao, W.-C.; Hosseini, D.; Stoian, D.; Chen, Z.; Abdala, P. M.; Copéret, C.; Müller, C. Structural insight into an atomic layer deposition (ALD) grown Al_2O_3 layer on Ni/SiO_2: impact on catalytic activity and stability in dry reforming of methane. *Catal. Sci. Technol.* **2021**, *11*, 7563−7577.
(54) Shahirah, M. N. N.; Gimbun, J.; Lam, S. S.; Ng, Y. H.; Cheng, C. K. Synthesis and characterization of a La Ni/α-Al_2O_3 catalyst and its use in pyrolysis of glycerol to syngas. *Renewable Energy* **2019**, *132*, 1389−1401.
(55) Farooqi, A. S.; Al-Swai, M.; Ruslan, F. H.; Mohd Zabidi, N. A.; Saidur, R.; Syed Muhammad, S. A. F.; Abdullah, B.; Abdullah, B. Catalytic conversion of greenhouse gases (CO_2 and CH_4) to syngas over Ni-based catalyst: Effects of Ce-La promoters. *Arab. J. Chem.* **2020**, *13* (6), 5740−5749.
(56) Singh, A.; Palakollu, V.; Pandey, A.; Kanvah, S.; Sharma, S. Green synthesis of 1, 4-benzodiazepines over La_2O_3 and $La(OH)_3$ catalysts: Possibility of Langmuir-Hinshelwood adsorption. *RSC Adv.* **2016**, *6* (105), 103455−103462.

(57) Yang, R.; Xing, C.; Lv, C.; Shi, L.; Tsubaki, N. Promotional effect of La_2O_3 and CeO_2 on Ni/γ-Al_2O_3 catalysts for CO_2 reforming of CH_4. *Appl. Catal., A* **2010**, *385* (1−2), 92−100.
(58) Valentini, A.; Carreño, N. L. V.; Leite, E. R.; Gonçalves R, F.; Soledade, L. E. B.; Maniette, Y.; Longo, E.; Probst, L. F. D. Improved activity and stability of Ce-promoted Ni/γ -Al_2O_3 catalysts for carbon dioxide reforming of methane. *Lat. Am. Appl. Res.* **2004**, *34*, 165−172.
(59) Alizadeh Sahraei, O.; Desgagnés, A.; Larachi, F.; Iliuta, M. C. Ni-Fe catalyst derived from mixed oxides Fe/Mg-bearing metallurgical waste for hydrogen production by steam reforming of biodiesel by-product: Investigation of catalyst synthesis parameters and temperature dependency of the reaction network. *Appl. Catal., B* **2020**, *279*, 119330.
(60) Vajglová, Z.; Gauli, B.; Mäki-Arvela, P.; Simakova, I. L.; Kumar, N.; Eränen, K.; Tirri, T.; Lassfolk, R.; Peurla, M.; Doronkin, D. E.; Murzin, D. Yu. Co-processing of fossil feedstock with lignin-derived model compound isoeugenol over Fe-Ni/HY-5.1 catalysts. *J. Catal.* **2023**, *421*, 101−116.
(61) Zhu, T.; Flytzani-Stephanopoulos, M. Catalytic partial oxidation of methane to synthesis gas over Ni-CeO_2. *Appl. Catal., A* **2001**, *208* (1−2), 403−417.
(62) Sagar, T. V.; Padmakar, D.; Lingaiah, N.; Rama rao, K. S.; Reddy, I. A. K.; Sai Prasad, P. S. Syngas production by CO_2 reforming of methane on $LaNi_xAl_{1-x}O_3$ perovskite catalysts: influence of method of preparation. *J. Chem. Sci.* **2017**, *129*, 1787−1794.
(63) Suo, C.; Liu, Y.; Zhang, X.; Wang, H.; Chen, B.; Fang, J.; Zhang, Z.; Chen, R.; Chen, R.; Shi, C. Embedded structure of Ni@PSi catalysts for steam reforming of methane. *Eur. J. Inorg. Chem.* **2022**, *2022*, No. e202200182.
(64) Zhang, Y.; Wang, W.; Wang, Z.; Zhou, X.; Wang, Z.; Liu, C. J. Steam reforming of methane over Ni/SiO_2 catalyst with enhanced coke resistance at low steam to methane ratio. *Catal. Today* **2015**, *256*, 130−136.
(65) Luisetto, I.; Tuti, S.; Romano, C.; Boaro, M.; Di Bartolomeo, E.; Kesavan, J. K.; Kumar, S. S.; Selvakumar, K. Dry reforming of methane over Ni supported on doped CeO_2: New insight on the role of dopants for CO_2 activation. *J. CO_2 Util.* **2019**, *30*, 63−78.
(66) Gao, N.; Cheng, M.; Quan, C.; Zheng, Y. Syngas production via combined dry and steam reforming of methane over Ni-Ce/ZSM-5 catalyst. *Fuel* **2020**, *273*, 117702−117714.
(67) Abbas, M.; Sikander, U.; Mehran, M. T.; Kim, S. H. Exceptional stability of hydrotalcite derived spinel Mg (Ni) Al_2O_4 catalyst for dry reforming of methane. *Catal. Today* **2022**, *403*, 74−85.
(68) Lanre, M. S.; Abasaeed, A. E.; Fakeeha, A. H.; Ibrahim, A. A.; Al-Awadi, A. S.; Jumah, A. . b.; Al-Mubaddel, F. S.; Al-Fatesh, A. S. Lanthanum-cerium-modified nickel catalysts for dry reforming of methane. *Catalysts* **2022**, *12*, 715−730.
(69) Aghamohammadi, S.; Haghighi, M.; Maleki, M.; Rahemi, N. Sequential impregnation vs. sol-gel synthesized Ni/Al_2O_3-CeO_2 nanocatalyst for dry reforming of methane: Effect of synthesis method and support promotion. *Mol. Catal.* **2017**, *431*, 39−48.
(70) Karam, L.; Armandi, M.; Casale, S.; El Khoury, V.; Bonelli, B.; Massiani, P.; El Hassan, N. Comprehensive study on the effect of magnesium loading over nickel-ordered mesoporous alumina for dry reforming of methane. *Energy Convers. Manage.* **2020**, *225*, 113470−113486.
(71) Ramon, A. P.; Li, X.; Clark, A. H.; Safonova, O. V.; Marcos, F. C.; Assaf, E. M.; van Bokhoven, J. A.; Artiglia, L.; Assaf, J. M. In situ study of low-temperature dry reforming of methane over $La_2Ce_2O_7$ and $LaNiO_3$ mixed oxides. *Appl. Catal., B* **2022**, *315*, 121528−121545.
(72) Figueredo, G. P.; Medeiros, R. L.; Macedo, H. P.; de Oliveira, A. A. S.; Braga, R. M.; Mercury, J. M. R.; Melo, M. A. F.; Melo, D. M. A. A comparative study of dry reforming of methane over nickel catalysts supported on perovskite-type $LaAlO_3$ and commercial α-Al_2O_3. *Int. J. Hydrogen Energy* **2018**, *43*, 11022−11037.
(73) Abdulrasheed, A. A.; Jalil, A. A.; Siang, T. J.; Hambali, H. U. Thermodynamic sensitivity analysis of CO_2 reforming of methane based on equilibrium predictions. *IOP Conf. Ser.: Mater. Sci. Eng.* **2020**, *808*, 012001.
(74) Ginsburg, J. M.; Piña, J.; El Solh, T.; de Lasa, H. I. Coke formation over a nickel catalyst under methane dry reforming conditions: Thermodynamic and kinetic models. *Ind. Eng. Chem. Res.* **2005**, *44* (14), 4846−4854.
(75) Li, S.; Fu, Y.; Kong, W.; Pan, B.; Yuan, C.; Cai, F.; Zhu, H.; Zhang, J.; Sun, Y. Dually Confined Ni nanoparticles by room-temperature degradation of AlN for dry reforming of methane. *Appl. Catal., B* **2020**, *277*, 118921−118932.
(76) Wang, N.; Shen, K.; Huang, L.; Yu, X.; Qian, W.; Chu, W. Facile route for synthesizing ordered mesoporous Ni-Ce-Al oxide materials and their catalytic performance for methane dry reforming to hydrogen and syngas. *ACS Catal.* **2013**, *3*, 1638−1651.
(77) Liang, T.-Y.; Chen, H. H.; Tsai, D. H. Nickel hybrid nanoparticle decorating on alumina nanoparticle cluster for synergistic catalysis of methane dry reforming. *Fuel Process. Technol.* **2020**, *201*, 106335−106347.

https://doi.org/10.1021/acs.iecr.3c02341
Ind. Eng. Chem. Res. 2023, 62, 20588−20607